NACA

26 NOV 1947

RESEARCH MEMORANDUM

WING-FLOW TESTS OF A TRIANGULAR WING OF ASPECT RATIO TWO.- I. EFFECTIVENESS OF SEVERAL TYPES OF TRAILING-EDGE FLAPS ON FLAT-PLATE MODELS

By George A. Rathert, Jr.,
and George E. Cooper

Ames Aeronautical Laboratory
Moffett Field, Calif.

NATIONAL ADVISORY COMMITTEE FOR AERONAUTICS

WASHINGTON

November 14, 1947

NACA RM No. A7G18

NATIONAL ADVISORY COMMITTEE FOR AERONAUTICS

RESEARCH MEMORANDUM

WING-FLOW TESTS OF A TRIANGULAR WING OF ASPECT RATIO TWO.- I. EFFECTIVENESS OF SEVERAL TYPES OF TRAILING-EDGE FLAPS ON FLAT-PLATE MODELS

By George A. Rathert, Jr.,
and George E. Cooper

SUMMARY

The problem of applying controls to low-aspect-ratio wings of triangular plan form has been investigated by means of the NACA wing-flow method using parallel-sided models having sharp leading and trailing edges. The control-effectiveness parameters $d\alpha/d\delta_f$ and $dC_m/d\delta_f$ were determined for $C_N = 0$ in the Mach number range from 0.50 to 1.10. Constant-chord and constant-percent-chord trailing-edge flaps, and triangular drooped-tip flaps were tested on a basic plan form of aspect ratio two, and semivertex angle of 26.6°. In all cases the flap area to total-area ratio was 0.20. The test Reynolds numbers varied from 500,000 to 1,300,000.

The low-speed results suggested that the inboard portion of the trailing edge was the most effective area for the location of a lift-producing flap-type control. At a Mach number of 0.50 the effectiveness of the constant-percent-chord flap was only about 10 percent less than that measured elsewhere in two-dimensional tests of a plain-flap straight-wing combination having an NACA 65-210 airfoil section.

Neither the basic plan form nor any of the control surfaces exhibited any critical stick-fixed characteristics in the transonic speed range within the range of normal-force coefficients tested, ±0.40. The flap effectiveness, both pitching-moment and lift-producing, dropped to about half the low-speed values near a Mach number of 1.0 and then began to recover. The plan-form normal-force curve slope and the location of the aerodynamic center did not vary appreciably with Mach number. The deflection of a constant-chord flap was slightly destabilizing but did not affect the lift-curve slope.

[redacted]

UNCLASSIFIED

The lift-producing effectiveness and plan-form characteristics of a 45° swept-back constant-chord flap on a modified plan form of the same aspect ratio and vertex angle were also measured and are presented in the report.

INTRODUCTION

The use of low-aspect-ratio wings of triangular plan form has been suggested in reference 1 and elsewhere as one means of achieving moderate supersonic speeds. Theoretical analyses of the lift and wave-drag characteristics at supersonic speeds are presented in references 2, 3, and 4. Very little information has been published, however, about the application of control surfaces to such a plan form. The present report is concerned with the relative effectiveness of different types of control surfaces, particularly in the transonic speed range.

A preliminary survey of this problem has been conducted by the NACA wing-flow method, which is described in reference 5. Simple half-span flat-plate models with sharp beveled leading and trailing edges were used. The lift and pitching-moment characteristics of three different types of trailing-edge and tip flaps were measured in the Mach number range from 0.50 to 1.10. The Reynolds number range was 500,000 to 1,300,000. The investigation was conducted on a triangular plan form of aspect ratio two, semivertex angle of 26.6°, using a flap-area to total-area ratio of 0.20. The plan form selected is the subject of a general coordinated research program on low-aspect-ratio wings now being conducted at the Ames Aeronautical Laboratory.

In order to permit qualitative comparison of the results obtained in the present tests with known trends (reference 6), a 45° swept-back constant-chord flap was tested on a modified plan form of the same aspect ratio and semivertex angle as the triangular wing.

SYMBOLS

The following symbols are used in this report:

A	aspect ratio (b^2/S)
b	full span, inches
C_m	pitching-moment coefficient $(2M'/qS\bar{c})$

C_N	normal-force coefficient $(2N/qS)$
$\bar{c}$	mean geometric chord, inches
H	test-station total pressure, pounds per square foot
H_o	free-stream total pressure, pounds per square foot
M	test station Mach number
M'	pitching moment acting on half-span model about the $\bar{c}/4$ axis, inch-pounds
N	normal force acting on half-span model, pounds
q	test-station dynamic pressure, pounds per square inch
S	full-span plan-form area, square inches
α	angle of attack, degrees
α_{FLOAT}	angle-of-attack data recorded by floating balance
δ_f	control-surface angle measured in a plane perpendicular to the hinge line, degrees
ϵ	plan-form semivertex angle, degrees
m	arc sin 1/M

TEST METHODS AND EQUIPMENT

Method

The half-span models were tested in the region of accelerated flow over the wing of a P-51B airplane and were mounted on small recording balances installed within the wing under the test stations. The desired control-effectiveness parameters were measured in two steps.

In the first series of tests the models were free to rotate to the angle of attack for zero pitching moment about a pivot axis on the balance. The normal-force coefficients were computed from simultaneous measurements of the floating angle and the pitching

moment about the model $\bar{c}/4$ axis. These measurements were made throughout the test range of Mach number for several deflections of each type of flap. The angle-of-attack and pitching-moment data were then corrected to zero-lift conditions using normal-force curve slopes determined by testing a representative model of each plan form on a three-component balance which was driven continuously to vary the angle of attack.

Models

A photograph of the series of models tested is presented in figure 1. The detailed dimensions are given in figure 2. Each model was fitted with an end plate of the type shown in figure 3 to minimize the effect of the slot cut in the test station skin to permit the model to rotate.

The control-flap angles were obtained by bending the models along the desired hinge lines. The edges of the flaps in the bent condition were straight within ±0.01 inch. The grooves machined near the hinge lines to provide relief for the bending operations were filled with putty, as can be seen in figure 1, and rubbed down to a smooth contour.

Balances

Two different types of recording balances were used during the tests. On the floating balance illustrated schematically in figure 4 the models were free to rotate about a pivot axis (A – A) ahead of the model leading edge. The angular position of the shaft A – A was recorded photographically by an optical system using a mirror mounted directly on the shaft. The pitching moment about axis B – B was measured by electrical strain gages on a cantilever arm restraining the shaft B – B in torsion. The strain-gage output was transmitted to a standard NACA recording galvanometer. The longitudinal position of the axis B – B was alined with the $\bar{c}/4$ point on each model.

The other balance used was a small three-component strain-gage balance which measured the normal force and pitching moment acting on the model continuously as the model was oscillated through a fixed angle-of-attack range at an average rate of 1.6° per second. The rotation was about a lateral axis passing through the quarter-chord point of the mean aerodynamic chord.

TEST STATION

Figure 5 is a photograph of the test station with a model installed. The square vane in the upper part of the photograph is a reference vane connected to a selsyn instrument which records the angle of inflow of the air stream over the test station. The difference in inflow between the reference vane and the test station was measured using a symmetrical vane on the model balance.

The characteristics of the air flow over the test station are summarized in figure 6, which includes the surface chordwise and the subsonic vertical Mach number distributions, and representative boundary-layer total-pressure profiles. The airplane spanwise velocity distributions were also measured and the gradients were found to be negligible.

The chordwise Mach number distributions (fig. 6(a)) were determined from a series of static-pressure measurements made at the test station with no model in place. These distributions were quite flat, precluding any significant chordwise differences in Mach number over the model area. The flat pressure distribution did tend to make the position of the main shock wave somewhat unstable at local Mach numbers of 1.00 to 1.05. Appearance of a shock wave on the test station was signaled by a definite unsteady shift in the inflow angle indicated by the reference vane, and data taken under such conditions were not used.

The vertical Mach number gradients at the test station were checked indirectly by measuring the spanwise distribution of local Mach number at the 60-percent-chord point on a 10-inch-high wedge-shaped airfoil located at the test station. The local Mach numbers (fig. 6(b)) were computed from measurements of the total and static pressure on the surface of the wedge. The indicated gradients correspond quite closely to the Mach number correction factor of 0.98 presented in reference 7 for use with a 5.69-inch-high model. For the present tests of a 3-inch-high model, a correction factor of 0.99 was applied to the triangular-tip flap data and no correction applied to the trailing-edge-type flap data.

The test station boundary-layer profiles (fig. 6(c)) were measured with a small total-head rake. The results indicate that the boundary layer should not have appreciably affected the air flow over the root portion of the models and flaps.

The variation of model Reynolds number with test station Mach number is presented in figure 7. The Reynolds numbers are based on

the mean geometric chords of the models, 4.0 inches for the triangular plan form and 3.25 inches for the swept-back plan form. The curves shown are average values, having been computed by assuming isentropic expansion to the test station from the NACA standard atmosphere at the test pressure altitude of 15,000 feet. Computed deviations from the curves of figure 6 caused by differences in the free-air temperature and the pressure altitude were found not to exceed ±5 percent.

ACCURACY

The detailed discussion of accuracy is confined to the accuracy of measurement of the various physical quantities presented as test data. There are several factors inherent in the wing-flow test technique which may largely affect the usefulness of the data for specific quantitative design purposes, principally the effects of the abnormally low Reynolds numbers. There are not, however, sufficient correlation data available at the present time to justify discussion in this report. Pending the availability of such data, the emphasis in the discussion has been placed on the qualitative results of the tests and the trends which are indicated.

Test Station

The evaluation of the test station Mach number and dynamic pressure is based on averaged measurements obtained during more than 50 check flights. Each of the test points was recorded during an individual constant Mach number dive to obtain as steady flow as possible over the test station. The variations from the data of figure 5(a) at any given airplane Mach number were found to be less than ±2 percent, and it is assumed that the same accuracy applies to the test flights with the models in place.

Floating Balance

The model angle of attack α_{FLOAT} was determined from three different measurements: the floating angle of the test balance, the inflow angle indicated by the reference vane, and the calibrated difference in inflow between the model station and the reference vane. The angular position of the test balance was recorded by a direct optical system with an error of -0.1° to $+0.3^{\circ}$.

This error includes that due to deflection of the pitching-moment gage, 0 to 0.2° for the range of pitching moment encountered. The position of the reference vane was recorded by a selsyn system with an over-all accuracy of ±0.5°. The difference in inflow between the test station and the reference vane varied about ±0.1°. The cumulative accuracy of the C_{FLOAT} data is therefore ±0.8°, which is a somewhat larger error than is actually indicated by the amount of scatter in the data. (See fig. 8.)

The accuracy of the floating-balance pitching-moment data is limited by the sensitivity of the recording galvanometer and the effect of ambient-temperature changes on the zero-load reading of the strain-gage electrical circuit. The correct zero reading was determined by repeating the flight-test procedure with no model in place. Agreement obtained on different flights at similar balance compartment temperatures indicates that this correction technique reduced the zero shift error to the order of a C_m of ±0.002 at a Mach number of 0.5. The remainder of the scatter indicated in figure 9 is attributed to insufficient galvanometer sensitivity.

Driven Balance

Angle-of-attack measurements in the driven balance are very similar to those of the floating balance discussed previously. The expected accuracy is the same, ±0.8°.

Strain-gage measurements of the normal force and pitching moment are subject to the same zero-shift correction discussed for the floating-balance pitching moments. The zero-shift errors in this case, again at a Mach number of 0.50, are equivalent to ±0.01 C_N and ±0.004 C_m.

Continuous oscillation of the model during the runs introduced another error in the form of hysteresis which can be observed by comparing the data for increasing and decreasing angles of attack in figures 10 and 11. This effect is very pronounced in the pitching-moment data. (See fig. 11.) It should be noted that the data are used in this report principally in the form of the slopes $dC_N/d\alpha$ and dC_m/dC_N and that these values are not affected by the direction of rotation of the model.

Due to a slight asymmetry of the normal-force gages about the neutral axis of the balance spindle, there was some interaction between drag and lift at high loads. In order to avoid errors

greater than ±0.01 in C_N, it was necessary to restrict the range of data presented to C_N of ±0.40.

RESULTS AND DATA ANALYSIS

Results

The measured variations of floating angle with Mach number at several different deflections for each type of flap are presented in figure 8. The corresponding values of C_m are given in figure 9. The driven balance force-test results are presented in figures 10 and 11 for the triangular plan form with constant-chord flap and in figures 12 and 13 for the swept-back plan form, $\delta_f = 0°$.

Data Analysis

The geometric characteristics of the floating balance, figure 7, indicate that the measured floating angle is actually the angle of attack for $C_N = (\bar{c}/4.3)\, C_m$. In order to obtain $d\alpha/d\delta_f$ at zero C_N, the α_{FLOAT} data were corrected to α for $C_N = 0 = C_L$ by the equation:

$$\alpha_{L_o} = \alpha_{FLOAT} - C_N \times \frac{1}{dC_N/d\alpha}$$

The normal-force coefficients were computed as $(\bar{c}/4.3) \times C_m$ from the data of figure 9. The normal-force curve slopes $dC_N/d\alpha$, which are presented in figures 14 and 15 as a function of Mach number, were determined from the data obtained on the driven balance. (See figs. 10 and 12.) An example of this correction procedure is presented in figure 16. The assumption has been made that $dC_N/d\alpha$ is a function of plan form only and is not affected by flap deflection. This assumption is supported by the data of figure 14 showing the normal-force curve slope unaffected by the constant-chord flap deflected 15.2°.

The correction to zero lift conditions outlined in the preceding paragraphs has been applied to the faired data of figure 8 at various increments of Mach number. The results are plotted in figure 17 as curves of α_{L_o} against flap angle at constant Mach number. The desired lift-effectiveness parameter $d\alpha/d\delta_f$ was read as the average slope between $\delta_f = 5°$ and 15°. These data are presented in figure 18 for each type of flap as a function of Mach number.

A similar procedure was used to determine the pitching-moment effectiveness $dC_m/d\delta_f$ for the triangular-plan-form controls. The pitching-moment slopes derived from the force-test data are presented in figure 19, $(C_{m_{\bar{c}/4}})_{C_L=0}$ against δ_f in figure 20, and $dC_m/d\delta_f$ as a function of Mach number in figure 21.

It will be noted from figure 19 that the constant-chord flap deflected 15.2° decreased the pitching-moment slope dC_m/dC_N about 0.011. This change has been extrapolated to the other required flap angles, and applied to the constant-percent-chord and triangular drooped-tip flaps as well. Due to the low values of C_N, the actual slopes used to correct the floating-balance data for the triangular drooped-tip flaps to zero C_N do not have an appreciable effect on the control-effectiveness slopes $d\alpha/d\delta_f$ and $dC_m/d\delta_f$.

DISCUSSION

Reynolds Number and Separation Effects

Before proceeding with the general discussion it is advisable to mention the very limited amount of data obtained on Reynolds number and separation effects. The Reynolds number range presented in figure 7 represents the maximum attainable with the models on the test airplane because of restrictions on the size of the flow field over the airplane wing and the minimum safe altitude for conducting the necessary dives. It was possible to reduce the Reynolds number by repeating flights at a higher test pressure altitude (25,000 ft), and this was done during the floating tests of the triangular drooped-tip flap deflected 18.4°. These test data, added to figure 8(a) using diamond symbols, correspond to Reynolds numbers of 500,000 to 1,000,000, rather than 700,000 to 1,300,000. There is no appreciable effect of Reynolds number in this very low range. All subsequent models were tested at 15,000 feet pressure altitude and the Reynolds numbers presented in figure 6.

In evaluating triangular or low-aspect-ratio plan-form data, it should be remembered that the Reynolds numbers are based on the mean aerodynamic chord length and therefore, under comparable test conditions, are considerably larger than those for more conventional straight wings of equal area.

In view of the possible importance of separation effects, one model, the triangular plan form with constant-chord flap, was tested first with the ridges caused by the bevels left sharp, and

then tested with the edges polished to a small radius. Although the actual extent of separation and the amount it was affected by rounding are unknown, there was no appreciable effect on the test results; all other models were tested in the rounded condition only.

Flap Effectiveness

Significant direct comparisons of control effectiveness are quite difficult to make when dealing with types of flaps having hinge lines of varying degrees of sweep. One of the best bases for comparing the relative effectiveness of different control surfaces would be the hinge moment required at the hinge line to produce a given increment of total lift or of pitching moment about a given axis. Such a comparison would, however, require the use of hinge-moment data, which is beyond the scope of the present tests.

The effectiveness parameter available from the test data is $d\alpha/d\delta_f$. The use of this parameter, however, is complicated by the fact that α is measured in a plane parallel to the relative wind; whereas δ_f is usually measured in a plane perpendicular to the hinge line. Thus, two flaps of equal area may produce equal increments of angle of attack when placed at the same angle with respect to the relative wind, but the numerical value of $d\alpha/d\delta_f$ for a highly swept flap will be considerably less than that for a straight flap. The swept flap, however, will have to be rotated through a greater angle at the hinge line to produce the desired relative wind angle, necessitating hinge-moment measurements to determine the relative efficiencies correctly.

In the present report both the parameters $d\alpha/d\delta_f$ and $dC_m/d\delta_f$ are presented with δ_f measured in a plane perpendicular to the hinge line. All comparisons in the following discussion have been made on this basis. If it is desired to compute the values of $d\alpha/d\delta_f$ or $dC_m/d\delta_f$ based on flap angles measured in a plane parallel to the free-stream direction, the necessary conversion factors $\left[(d\alpha/d\delta_f)_{\text{relative wind}} = \text{conversion factor} \times (d\alpha/d\delta_f)_{\text{hinge line}}\right]$ to be applied to the summary data of figures 18 and 21 are presented in the following table:

Type of control	Conversion factor
Constant chord	1.00
Constant percent chord	1.08
Triangular drooped tip	2.25
45° swept back	1.41

Lift effectiveness.- The data presented in figure 18 show that the constant-percent-chord flap is the most effective triangular plan-form control at low speeds: $d\alpha/d\delta_f = -0.46$ at a Mach number of 0.50, followed by the constant-chord flap, −0.42, and the triangular drooped-tip flap, −0.27. The relative positions of the constant-chord and constant-percent-chord flaps immediately suggest that the inboard portion of the trailing edge is the most effective area for the location of lift-producing flap-type controls at subsonic speeds.

Both the constant-percent-chord and the constant-chord flaps appear to possess acceptably high effectiveness at low speeds on the basis of the comparison presented in figure 18 with a constant-chord flap on a straight wing. The value of $d\alpha/d\delta_f$ obtained at a Mach number of 0.50 with the constant-20-percent-chord flap is only 10 percent less than that measured in the two-dimensional tests of a 20-percent-chord plain flap on an NACA 65-210 airfoil section reported in reference 8. The effectiveness of the 45° swept-back flap, also presented in figure 18, is comparatively low, −0.25 at a Mach number of 0.5.

At higher Mach numbers all three triangular plan-form controls lose effectiveness gradually, dropping to a minimum of about 55 percent of their low-speed effectiveness near a Mach number of 1.0. This gradual deterioration is in marked contrast with the behavior of the plain-flap straight-wing combination, which loses effectiveness very rapidly above a Mach number of 0.82.

At still higher speeds, above a Mach number of 1.00, the triangular plan-form controls begin to recover effectiveness. The constant-chord and triangular drooped-tip flaps recover quite

rapidly to 70 percent of their low-speed effectiveness at a Mach number of 1.075.

As would be expected the drop in effectiveness of the 45° swept-back flap is delayed to about a Mach number of 1.0. There is no evidence of the recovery noted on the triangular plan-form controls; however, it seems reasonable to assume that it would probably occur above the highest Mach number which could be reached in the tests, 1.10.

Although the variation of angle of attack with flap angle, shown in figure 17, is linear in the range (δ_f = 5° to 15°) used in preparing figure 18, it is obvious that the curves of figure 17 will not be linear in some small range on either side of zero flap angle. The explanation of this result has not been determined. A similar type of data showing the same behavior may be observed in figure 6 of reference 6. The random variations in the sequence of test Mach numbers and the fact that each flap angle was tested on separate flights rule out the possibility of progressive experimental errors or zero shifts.

In view of the definition of flap angle as measured in a plane perpendicular to the hinge line rather than parallel to the free-stream direction, it is interesting to note in figure 17 that both the constant-chord and the triangular drooped-tip flaps begin to lose effectiveness at about the same flap angle, 15°. Up to a Mach number of 0.60 the constant-percent-chord flap characteristics remain linear at 20.7°, the highest flap angle tested.

Above a Mach number of 1.00 the constant-chord and triangular drooped-tip flap characteristics become linear at the highest angles tested; whereas those of the constant-percent-chord flap begin to fall off at δ_f = 15°. It will be noted from figure 18 that the tendency to recover the low speed $d\alpha/d\delta_f$ also was less pronounced with this flap.

Pitching-moment effectiveness.— The ability of the three triangular plan-form controls to produce a change in pitching moment about the $\bar{c}/4$ (50-percent-root chord) axis is summarized in figure 21. The characteristics are very similar to the lift effectiveness discussed previously except that the minimum effectiveness occurs at slightly lower Mach numbers and the tendency to recover at supersonic speeds is more pronounced. The data do not indicate sufficient differences in effectiveness between the constant-chord and constant-percent-chord flaps to provide any basis for selecting the best type of control.

Figure 22, which is a reproduction of figure 7 of reference 7 with some of the present results added, summarizes indications of the effectiveness at transonic speeds of several types of controls and plan forms by comparing the floating angles in the transonic speed range with the floating angle at a Mach number 0.70. Again the figure emphasizes the contrast between the gradual moderate loss in effectiveness and subsequent recovery of the triangular plan-form controls, and the rapid and very severe changes experienced by the straight-wing plain-flap and dive-recovery flap combinations. Also in figure 22, the swept-flap results (item (5)) are compared with those obtained during other wing-flow-method tests (reference 6) of a similar configuration with a 14.1° semivertex angle (item (1)). The qualitative agreement is good, although the present test configuration loses more effectiveness than that of the referenced tests. This could be attributed to the slightly different plan form of the model of reference 6.

Plan-form Characteristics

Triangular wing.— The variations of normal-force curve slope $dC_N/d\alpha$ and the pitching-moment slope dC_m/dC_N with Mach number are presented in figures 14 and 19, respectively. It will be noted from figures 10 and 11 that the normal force and pitching moment vary linearly with angle of attack throughout the limited test range.

The value of normal-force curve slope is quite high, 0.055, and does not vary with Mach number through the range of the tests, 0.57 to 1.05. A slope of only 0.045 is indicated by the potential-flow theory of reference 9. As reported in reference 10, a 25-foot-span model of identical plan form with a symmetrical 5-percent-thick double-wedge airfoil section has been tested and a lift-curve slope of 0.040 obtained.

The theoretical slopes computed according to Jones (reference 1) and Brown (reference 2) have been added to figure 14 as a matter of interest, although the excellent agreement is not too significant in view of the limitations expressed in reference 1 with respect to the magnitude of the semivertex angle and in reference 2 with respect to the Mach number. In reference 11 an experimental criterion for the high Mach number limit of applicability of the lift-curve slope derived in reference 1, $dC_L/d\alpha = 2\pi \tan \epsilon$, is presented in the form $\tan \epsilon / \tan m = 0.30$. (See fig. 14.) This criterion indicates that Jones' derivation should apply throughout the range of test

Mach numbers. The tests of reference 11, however, were conducted at higher Mach numbers; consequently, the vertex angle at the critical value of tan ϵ/tan m was smaller and more nearly approximated the assumptions expressed in reference 1 than did the present models.

The pitching-moment slopes (fig. 19) indicate that the aerodynamic center was at approximately 36 percent $\bar{c}$. This agrees very well with the low-speed position of 37 percent $\bar{c}$ measured in the previously discussed tests of reference 10. The deflection of the constant-chord flap 15.2° was slightly destabilizing, moving the aerodynamic center forward 1 percent. The position of the aerodynamic center did not change appreciably with Mach number, so that no critical plan-form characteristics were observed at low lift coefficients in the transonic speed range.

This presentation of plan-form characteristics has been limited to a C_N range of ±0.40 in order to remain within the stated accuracy limits. That these results should not be extrapolated to higher lift coefficients is definitely indicated by the discussion of low-speed tests presented in reference 10. It was shown in this reference that, at lift coefficients of approximately 0.6 to 0.8, there was considerable separation of flow on the sharp leading edges of the wing, resulting in distinct breaks in the moment and force variations with angle of attack in such a way as to reduce the trailing-edge flap-control effectiveness. A discussion of the effect of this flow separation on the lift-producing effectiveness of a constant-chord split flap is included in the reference. Leading-edge separation in the case of a two-dimensional wedge-shaped airfoil has been discussed in reference 12.

Swept-back wing.— Figure 15 shows that the normal-force curve slope drops off very slowly from 0.044 at low speeds to 0.041 at a Mach number of 1.03 and then falls off more rapidly to 0.035 at a Mach number of 1.1. It is noteworthy that these data do not indicate any increase in normal-force curve slope at high subsonic Mach numbers.

The pitching-moment slopes (fig. 23) again show little change with Mach number up to a Mach number of 1.03. The aerodynamic center almost coincides with the center of area. Above a Mach number of 1.03 the aerodynamic center moves farther aft and is at 55 percent $\bar{c}$ at a Mach number of 1.10. Although the qualitative variation is reasonable, the aerodynamic center location seems to be considerably farther aft than comparison with the triangular plan form would indicate.

[redacted]

Angle of Zero Lift

The angle of zero lift of the triangular plan form with the constant-chord flap deflected changed considerably with Mach number. This variation is shown in figure 24 using results from both the force tests and the floating-angle tests to demonstrate that the shift was not a peculiarity of one or the other test method. A similar shift is apparent in all of the floating-angle data (fig. 8) for the control surfaces tested on the triangular plan form. The equivalent shift in the pitching moment at zero lift is shown in figure 25.

Triangular Plan-Form Flying-Wing Characteristics

The results of the present tests have been used to estimate some of the characteristics of a hypothetical flying-wing airplane of triangular plan form with a constant-chord flap for longitudinal control. A center-of-gravity position at 25 percent $\bar{c}$ and level flight at 40,000 feet altitude with a wing loading, of 45 pounds per square foot have been assumed.

Figure 26 presents the variation of pitching-moment coefficient with normal-force coefficient at four flap angles for several Mach numbers. In figure 27, these data have been cross-plotted at the trim normal-force coefficient corresponding to each Mach number. Since the models were symmetrical, it has been assumed that up-flap deflection produced an equal pitching-moment change of opposite sign to that measured for an equal down-flap deflection. The curves of figure 27 are broken in the range around $\delta_f = 0^\circ$ where C_m apparently does not vary linearly with δ_f.

The variation of flap angle required for balance with Mach number, determined from the $C_m = 0$ intercepts on figure 27, is presented in figure 28. The total change in elevator angle required for balance in the Mach number range from 0.70 to 1.075 is less than 2°. There do not appear to be any stick-fixed-control characteristics in the Mach number and lift-coefficient range covered which would be critical in the design of the longitudinal-control system.

CONCLUSIONS

The conclusions formed during this preliminary survey of the problem of applying control surfaces to low-aspect-ratio wings of

triangular plan form in the normal-force-coefficient range ±0.40 may be summarized as follows:

1. The inboard portion of the trailing edge was the most effective area tested for the location of a lift-producing flap-type control at subsonic speeds. (In defining the effectiveness, the flap angle was measured in a plane perpendicular to the hinge line.)

2. Both constant-chord and constant-percent-chord trailing-edge flaps appeared to have satisfactory lift-producing effectiveness at low speeds when compared to a plain-flap straight-wing combination of equal flap area to total-area ratio.

3. All three triangular plan-form controls exhibited moderate transonic characteristics, gradually losing about half of their low-speed effectiveness near a Mach number of 1.0 and then recovering at higher speeds.

4. Neither the plan-form lift-curve slope nor the location of the aerodynamic center changed appreciably from Mach numbers of 0.54 to 1.07. Deflection of a constant-chord flap had a slightly destabilizing effect but did not change the lift-curve slope.

5. The test results did not indicate any critical stick-fixed longitudinal-control characteristics from Mach numbers of 0.50 to 1.10 within the range of $C_N = \pm 0.40$ which would furnish a basis for selecting the type of control to be used on a given design.

Ames Aeronautical Laboratory,
National Advisory Committee for Aeronautics,
Moffett Field, Calif.

REFERENCES

1. Jones, Robert T.: Properties of Low-Aspect-Ratio Pointed Wings at Speeds Below and Above the Speed of Sound. NACA TN No. 1032, 1946.

2. Brown, Clinton E.: Theoretical Lift and Drag of Thin Triangular Wings at Supersonic Speeds. NACA TN No. 1183, 1946.

3. Puckett, Allen E.: Supersonic Wave Drag of Thin Airfoils. Jour. of Aero. Sci., vol. 13, no. 9, Sept. 1946, pp. 475-484.

4. Stewart, H. J.: The Lift of a Delta Wing at Supersonic Speeds. Quart. of Appl. Math., vol. 4, no. 3, Oct. 1946, pp. 246-254.

5. Gilruth, R. R., and Wetmore, J. W.: Preliminary Tests of Several Airfoil Models in the Transonic Speed Range. NACA ACR No. L5E08, 1945.

6. Daum, Fred L., and Sawyer, Richard H.: Tests at Transonic Speeds of the Effectiveness of a Swept-Back Trailing-Edge Flap on an Airfoil Having Parallel Flat Surfaces, Extreme Sweepback, and Low Aspect Ratio. NACA CB No. L5H01, 1945.

7. Silsby, Norman S., and Daum, Fred L.: The Effectiveness of a Trailing-Edge Spoiler on a Swept-Back Airfoil at Transonic Speeds From Tests by the NACA Wing-Flow Method. NACA CRM No. L6K12a, 1946.

8. Stivers, Louis S.: The Effectiveness at High Speeds of a 20-Percent-Chord Plain Trailing-Edge Flap on the NACA 65-210 Airfoil Section. NACA CRM A7A17, 1947.

9. Krienes, Klaus: The Elliptic Wing Based on the Potential Theory. NACA TM No. 971, 1941.

10. Anderson, Adrien E.: An Investigation at Low Speed of a Large-Scale Triangular Wing of Aspect Ratio Two.- I. Characteristics of a Wing Having A Double-Wedge Airfoil Section With Maximum Thickness at 20-Percent Chord. NACA RRM No. A7F06, 1947.

11. Ellis, Macon C., Jr., and Hasel, Lowell E.: Preliminary Tests at Supersonic Speeds of Triangular and Swept-back Wings. NACA CRM No. L6L17, 1947.

12. Lindsey, W. F., Daley, Bernard N., and Humphreys, Milton D.: The Flow and Force Characteristics of Supersonic Airfoils at High Subsonic Speeds. NACA TN No. 1211, 1947.

[redacted]

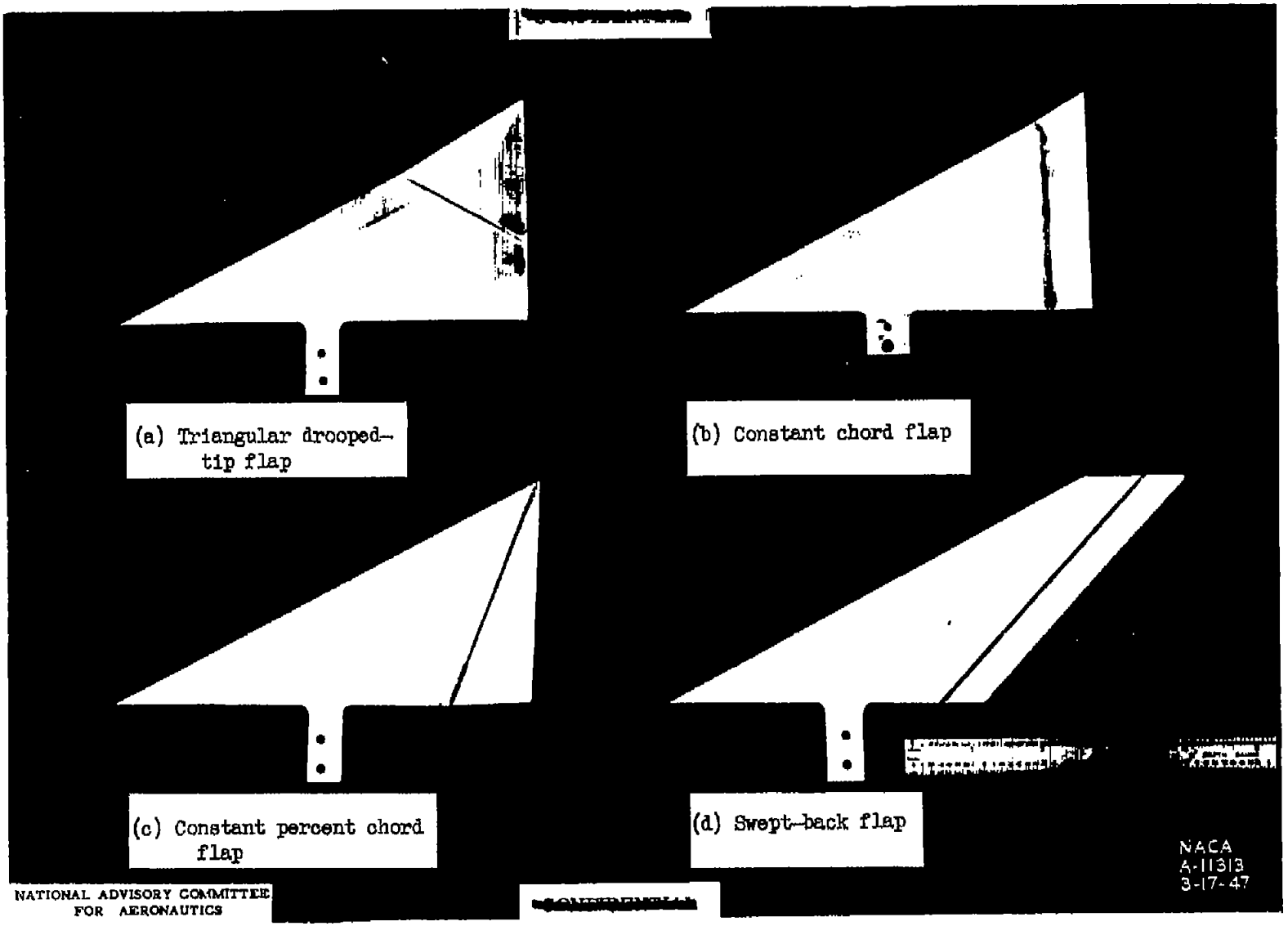

Figure 1.- Low-aspect-ratio wing-control model series.

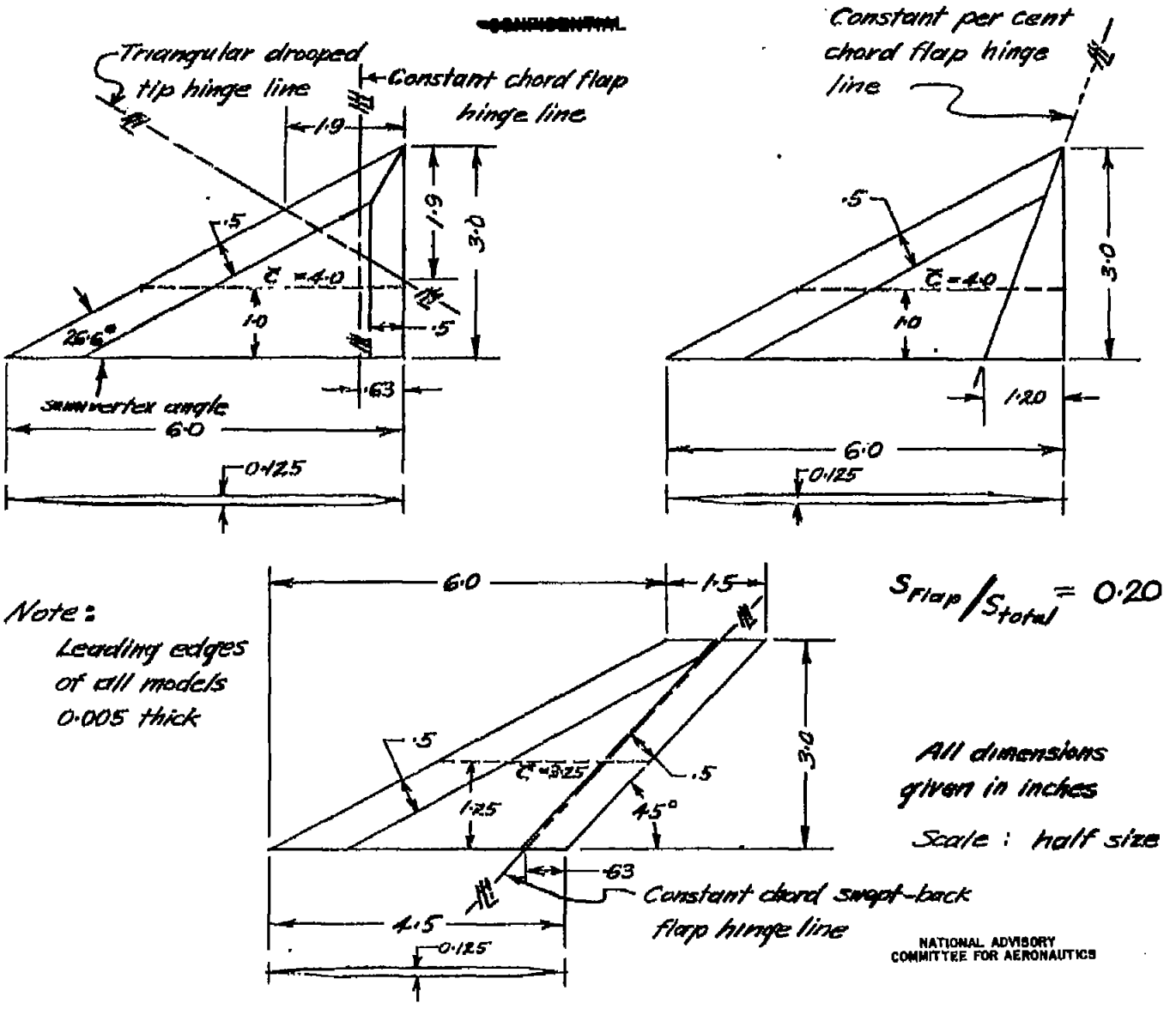

Figure 2.— Detail dimensions of the low aspect ratio wing control model series. CONFIDENTIAL

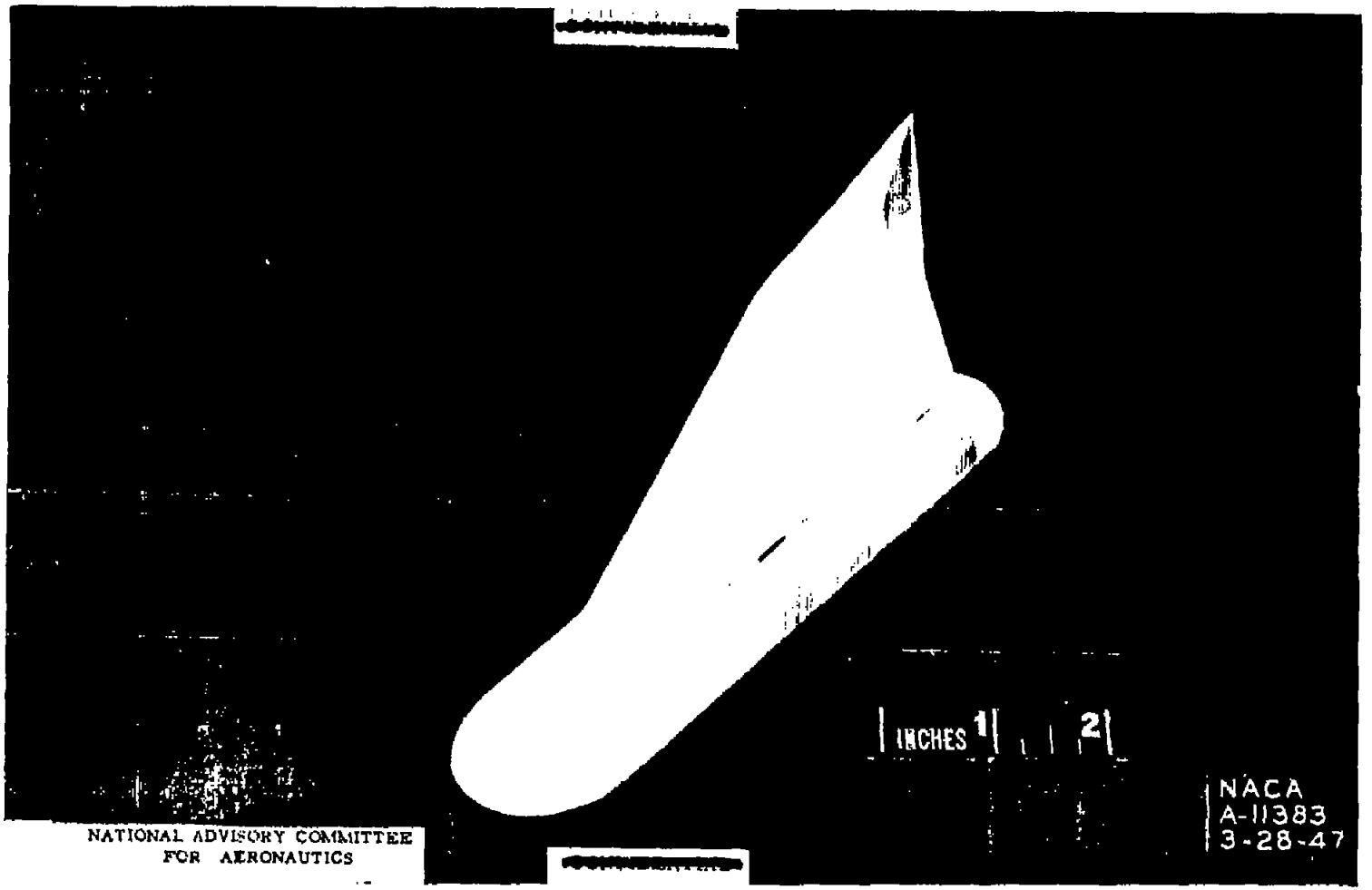

Figure 3.– Low-aspect-ratio wing-control model with end plate attached.

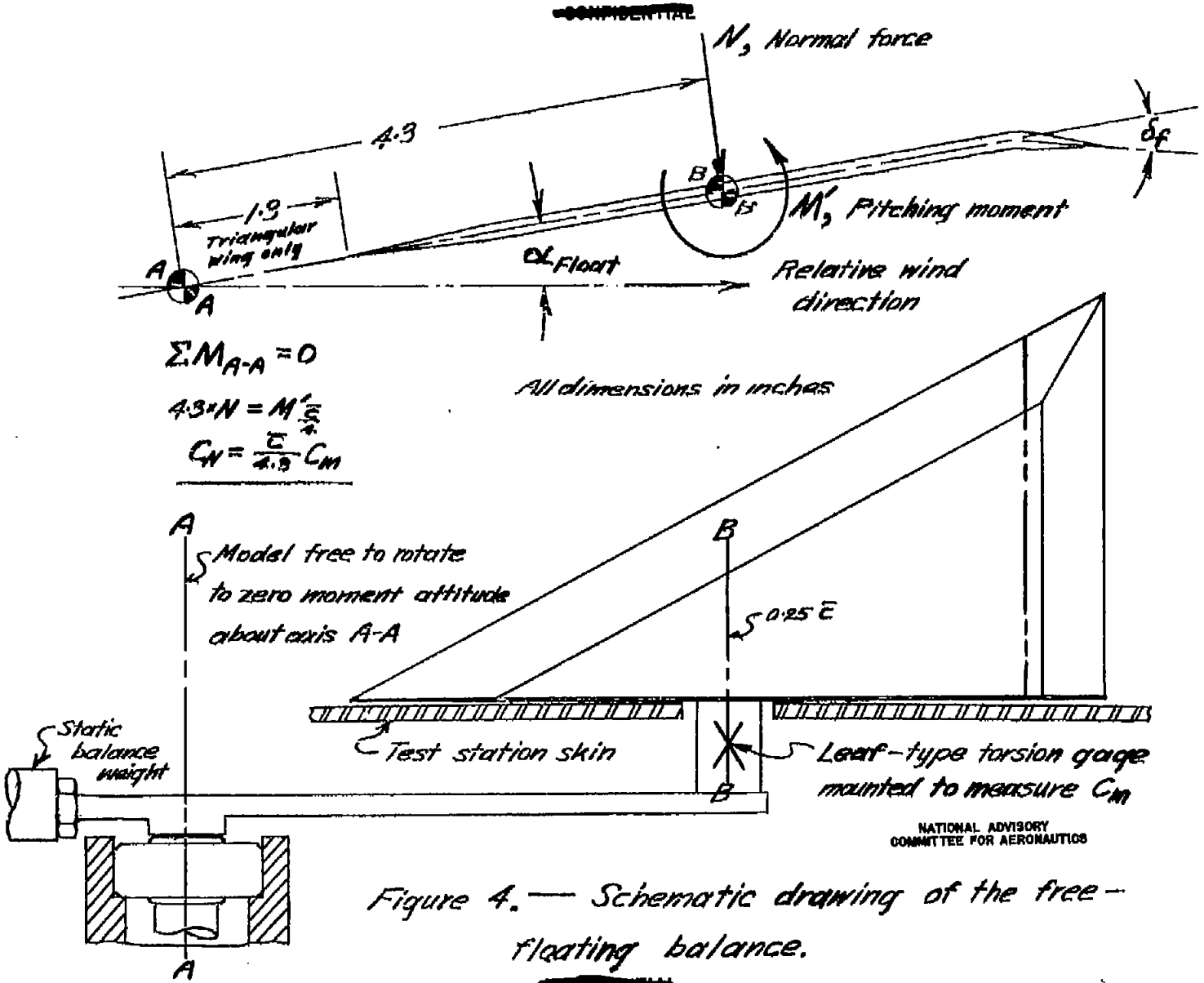

Figure 4.— Schematic drawing of the free-floating balance.

CONFIDENTIAL

Figure 5.- Wing-flow-method test station with low-aspect ratio wing-control model installed.

CONFIDENTIAL

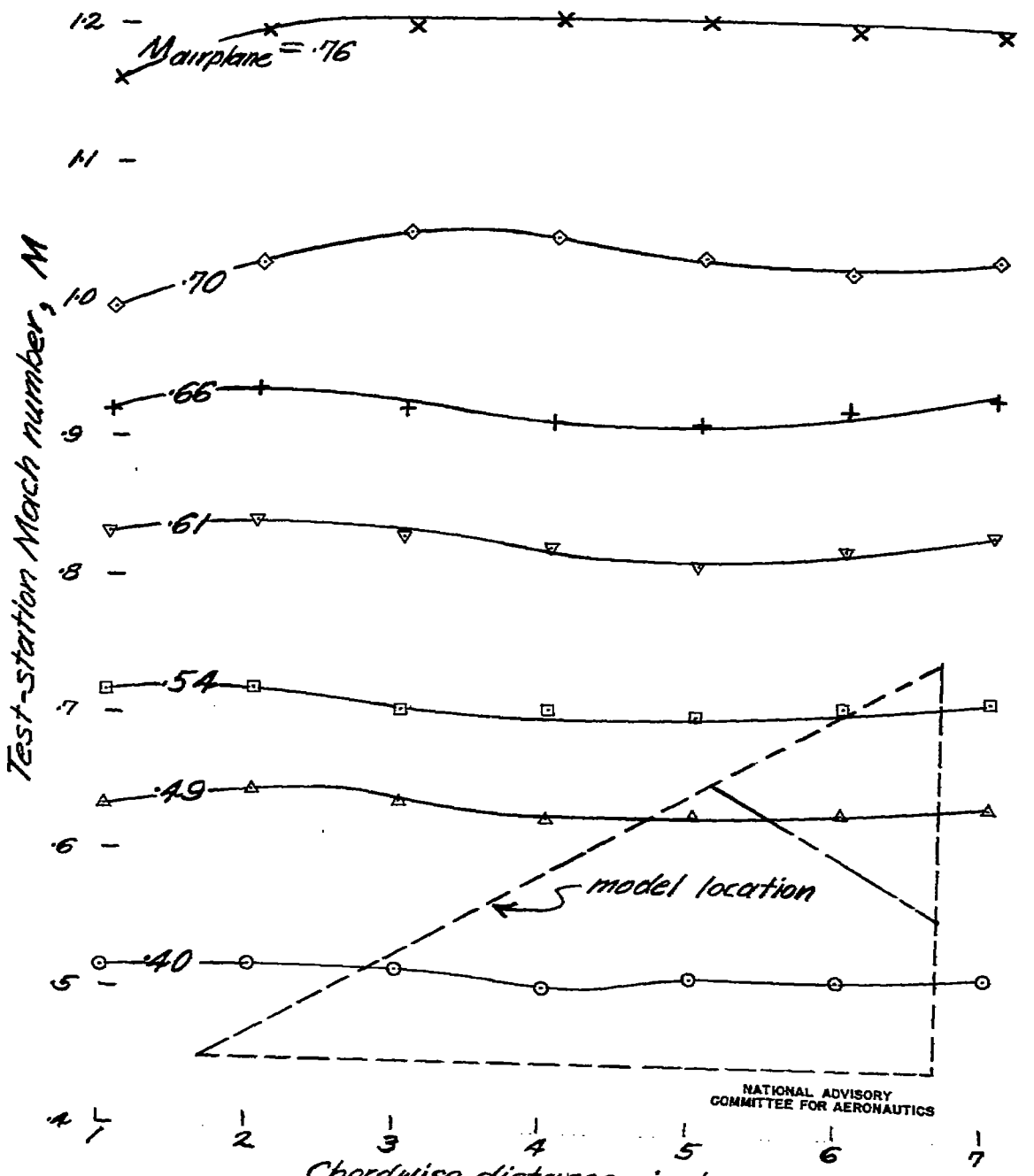

(a) Typical chordwise Mach number distributions

Figure 6. —— Test station characteristics.

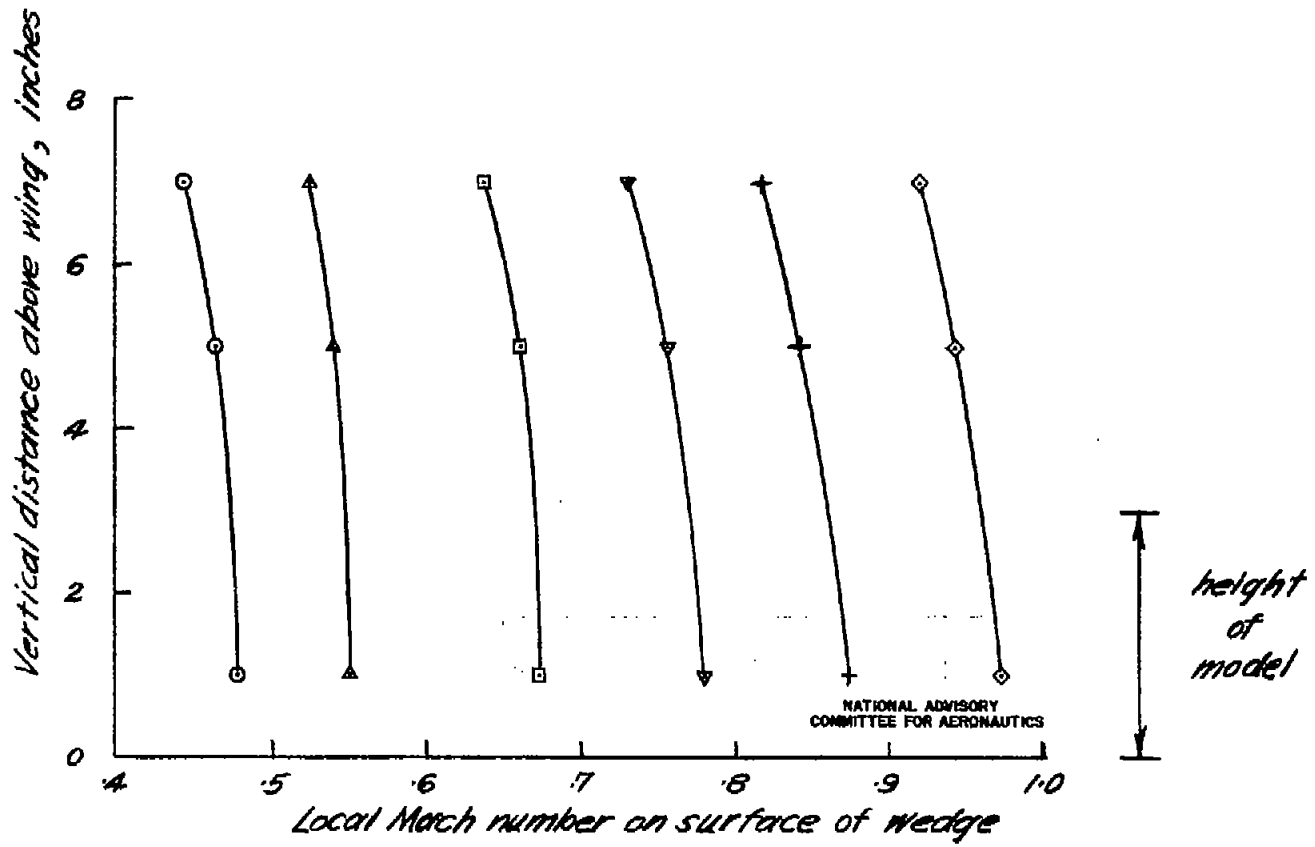

(b) Typical vertical Mach number distributions obtained by measuring pressure at 60% chord point on a wedge airfoil located at the test station

Figure 6. —— continued

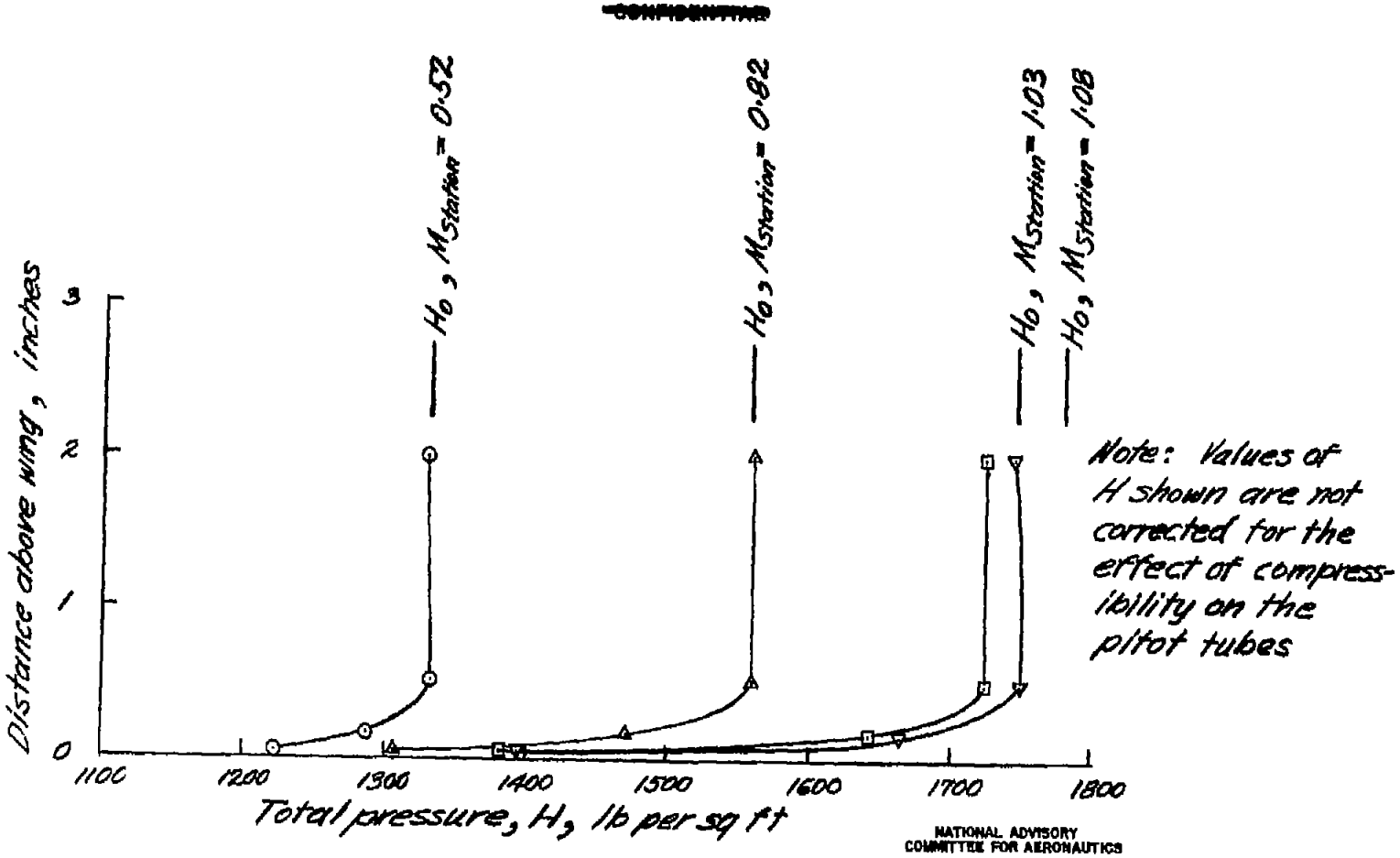

(c) Typical boundary-layer profiles as measured at the test station for several test station Mach numbers

Figure 6.— concluded.

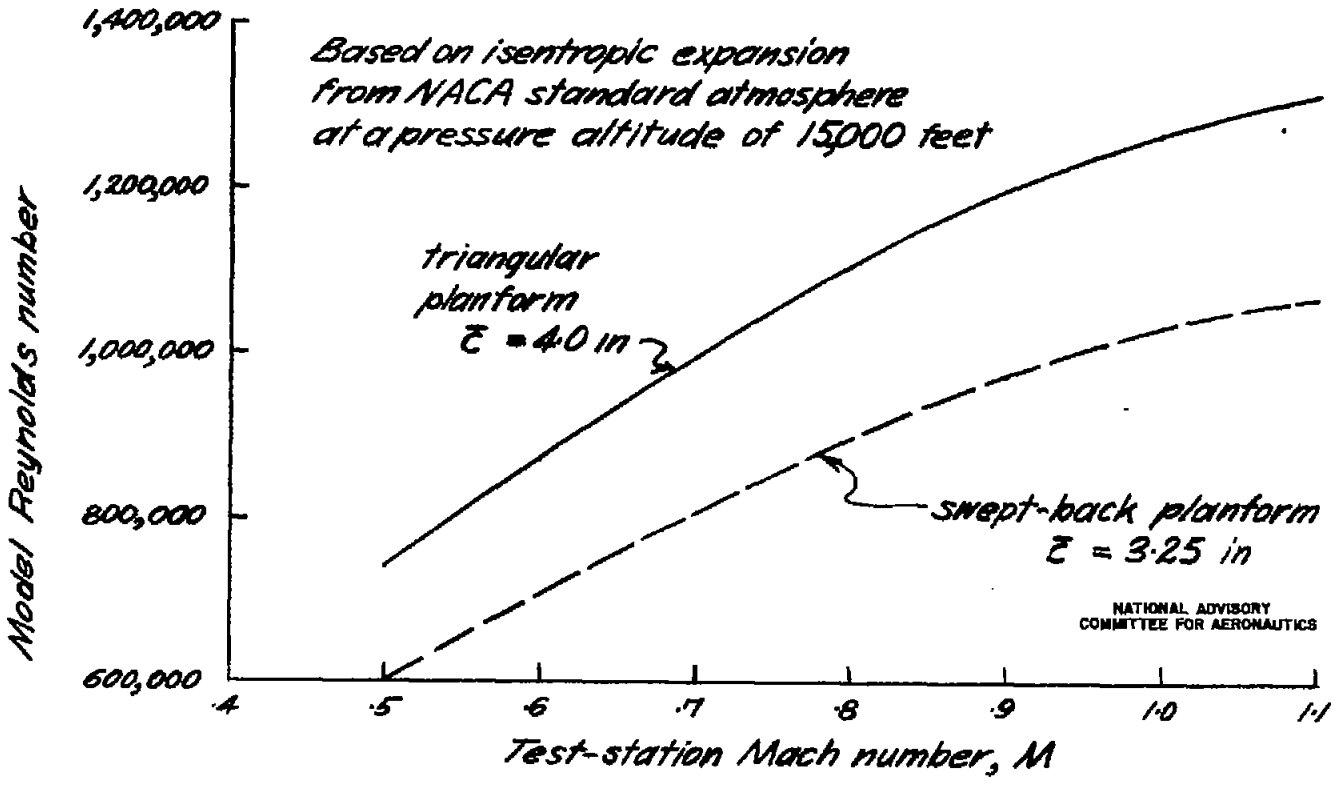

Figure 7. —— The variation of average model Reynolds number with test-station Mach number.

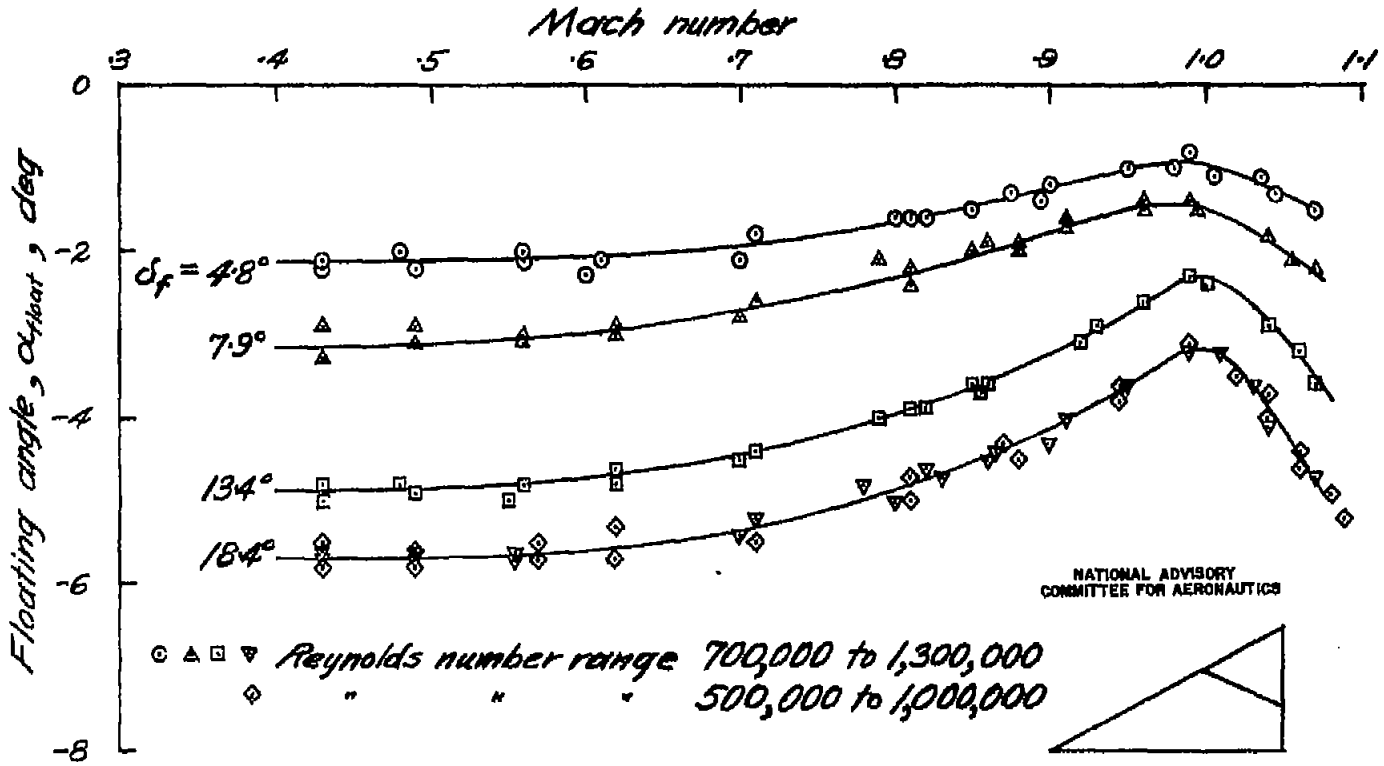

(a) Triangular drooped-tip flap

Figure 8. —— The variation of floating angle, α_{float}, with Mach number for several different flap angles.

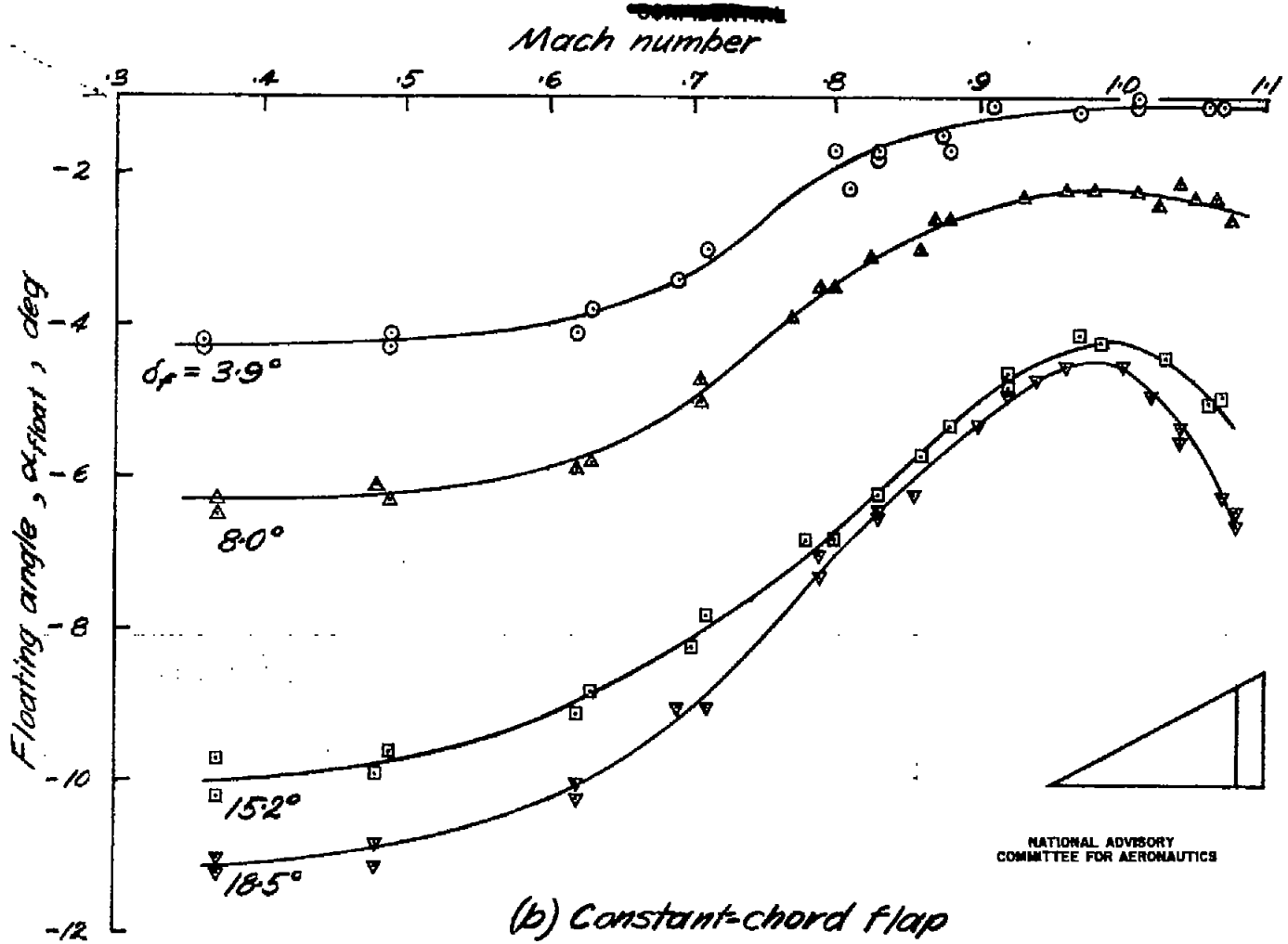

(b) Constant-chord flap

Figure 8. —— continued

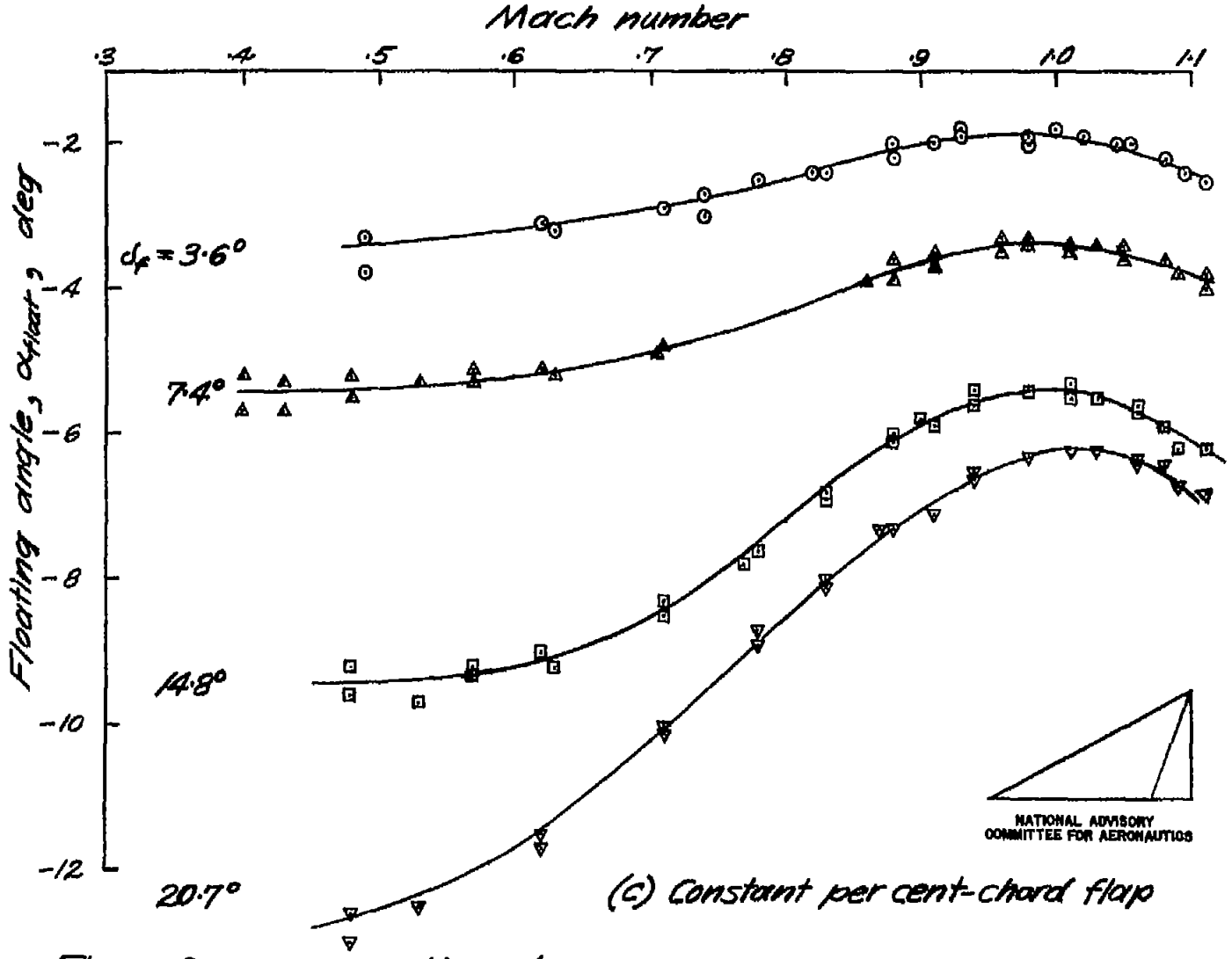

(c) Constant per cent-chord flap

Figure 8. —— continued

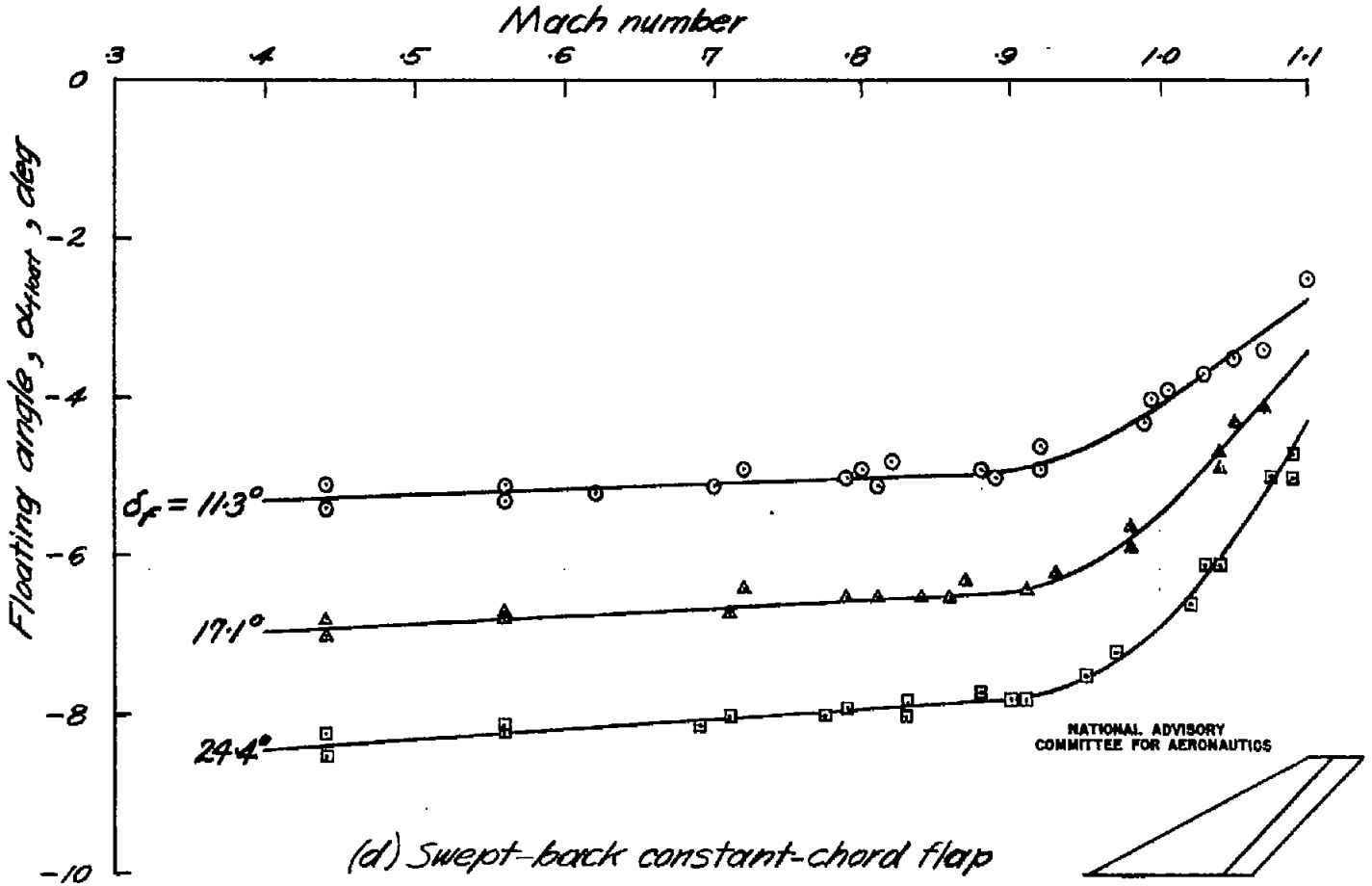

(d) Swept-back constant-chord flap

Figure 8. — concluded.

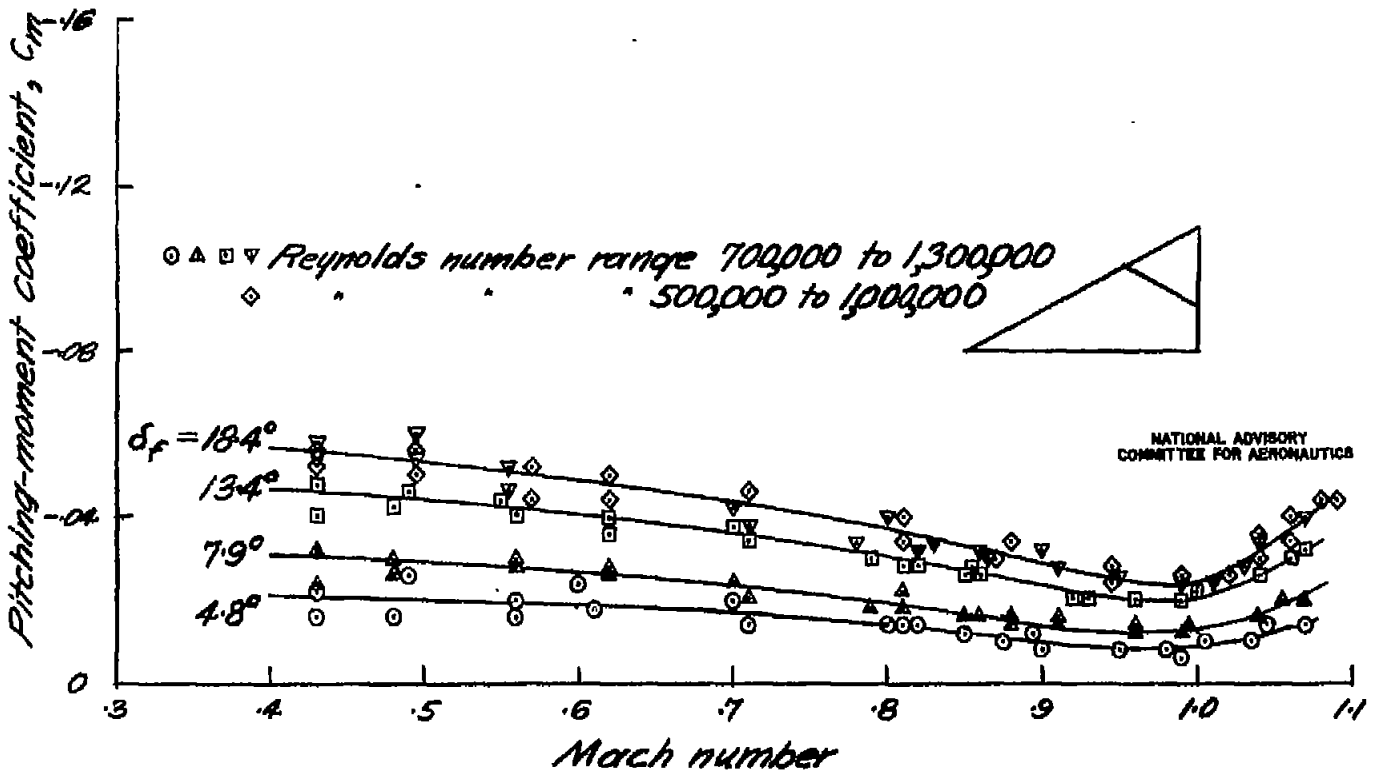

(a) Triangular drooped-tip flap

Figure 9. ——— Variation of C_m with Mach number measured during floating angle tests at several different flap angles. ———

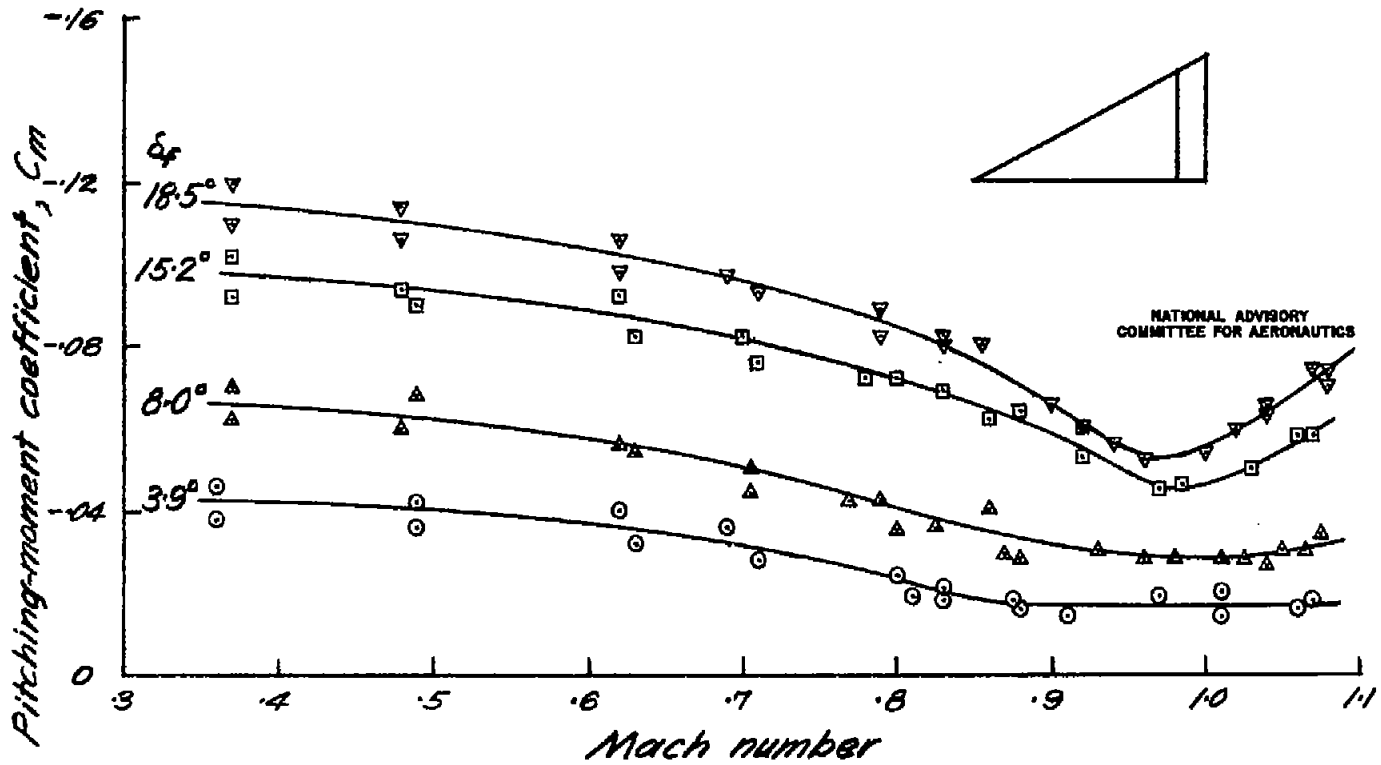

(b) Constant-chord flap

Figure 9. —— continued

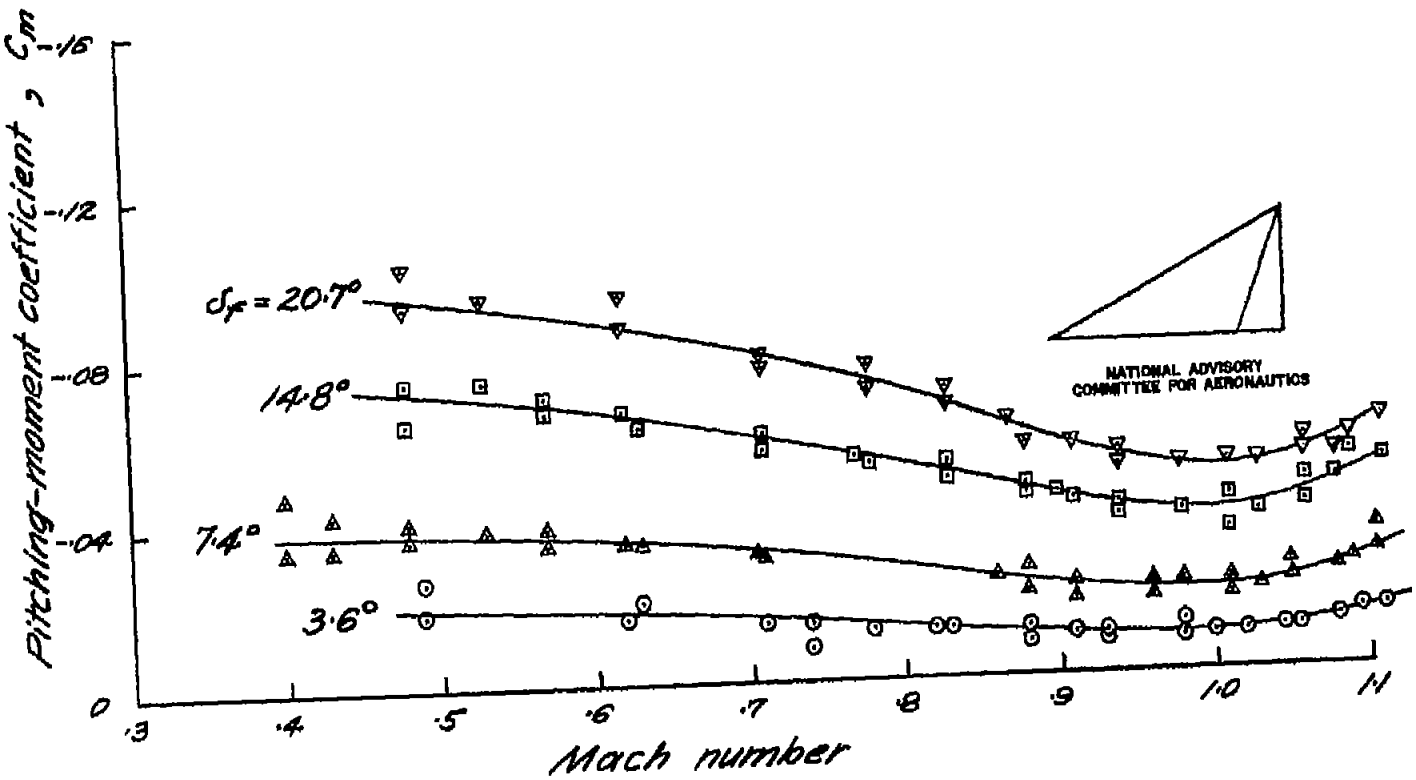

(c) Constant per cent-chord flap

Figure 9. —— continued

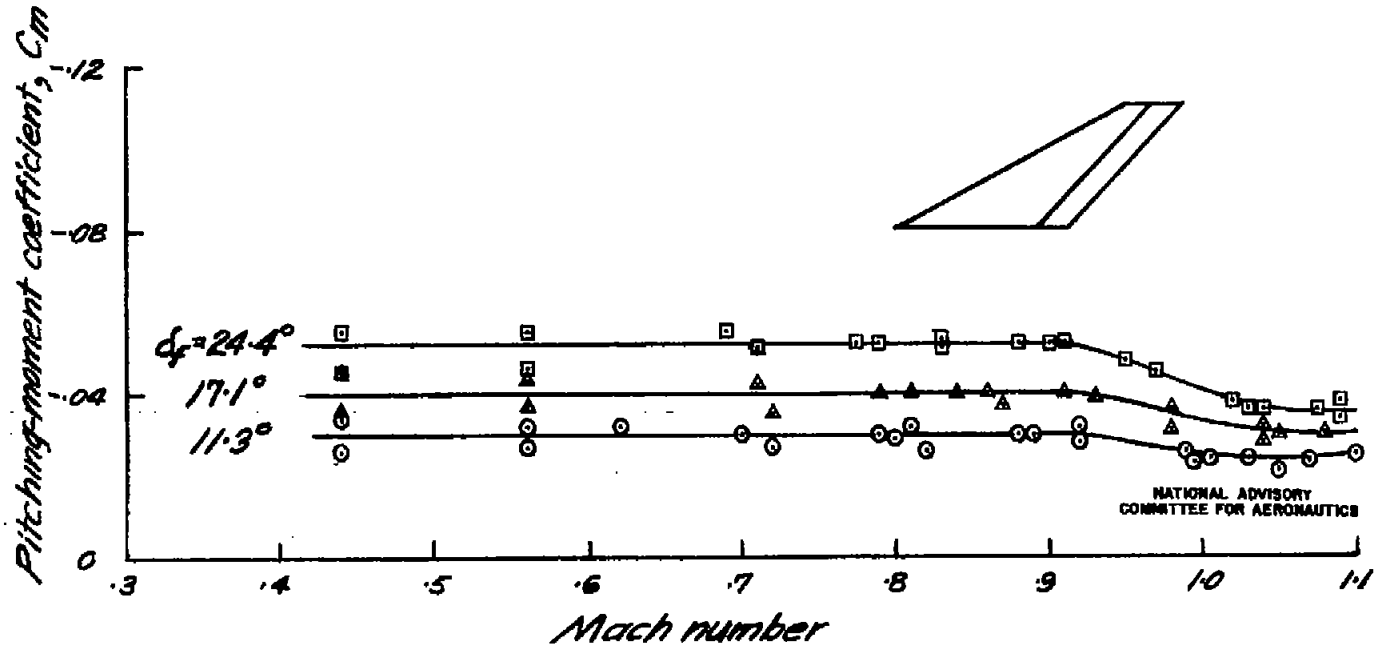

(d) Swept-back constant-chord flap

Figure 9 .—— concluded.

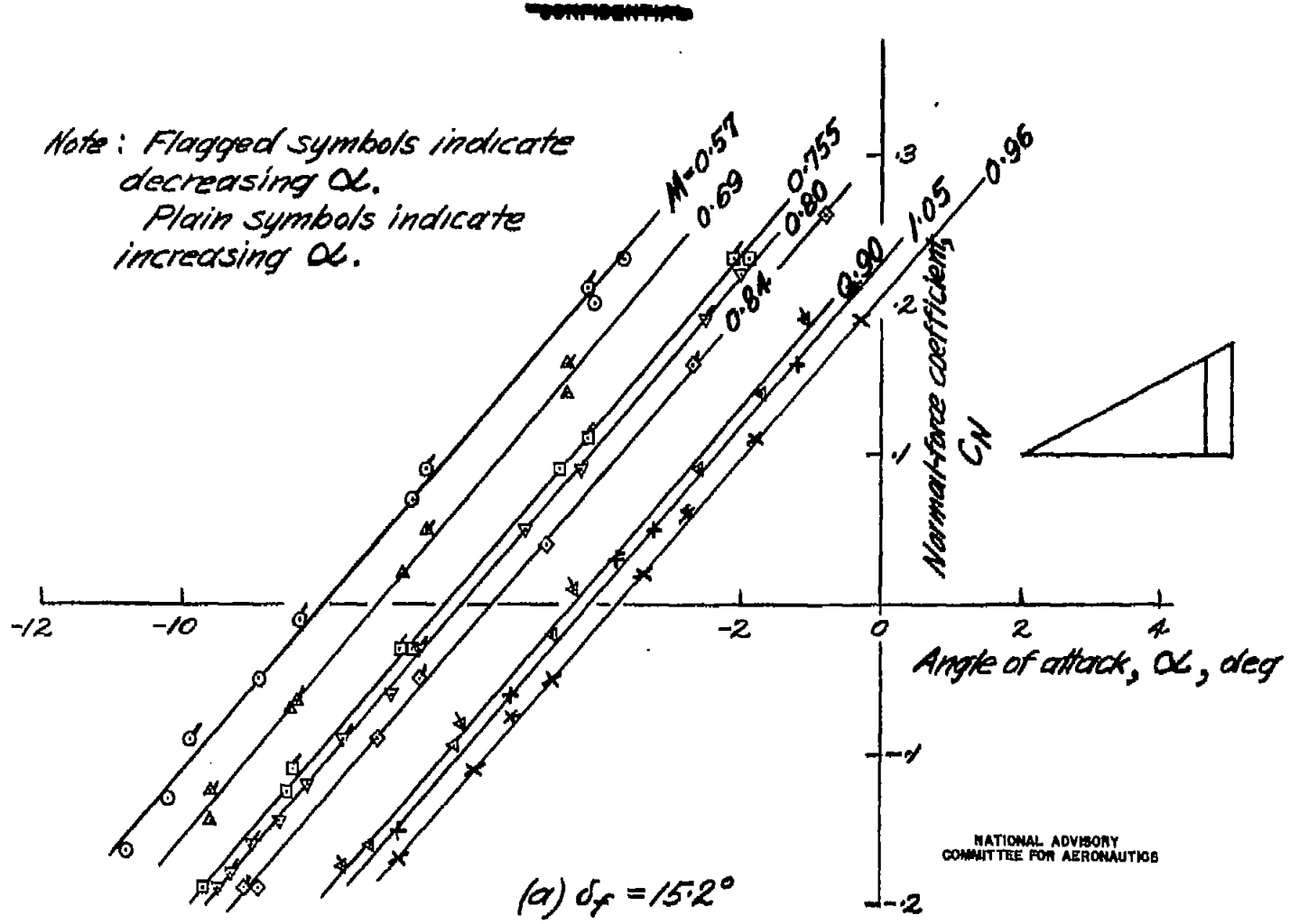

Figure 10. —— Variation of normal-force coefficient with angle of attack at various Mach numbers for triangular wing with constant-chord flap.

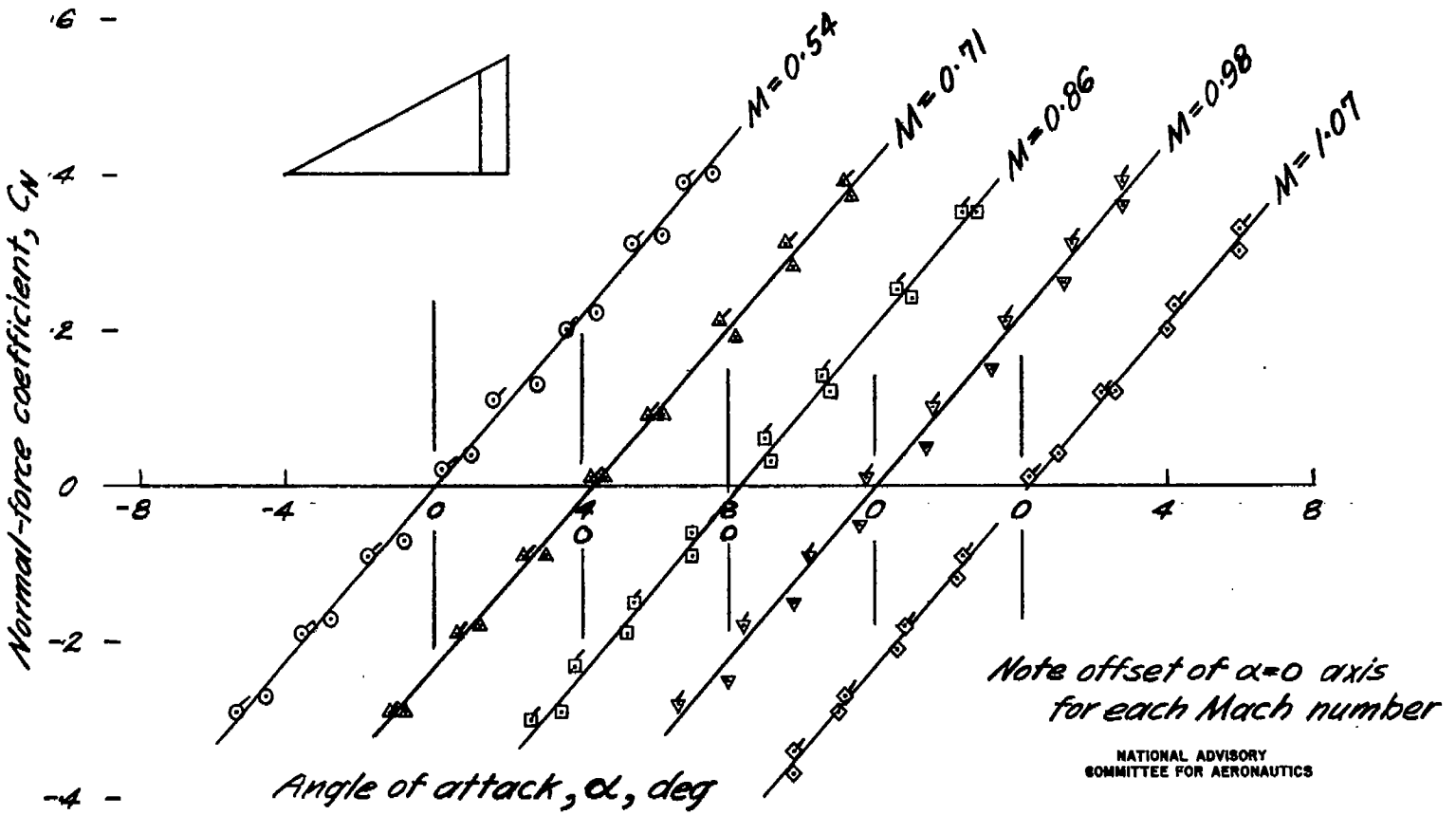

(b) $\delta_f = 0°$

Figure 10. —— concluded.

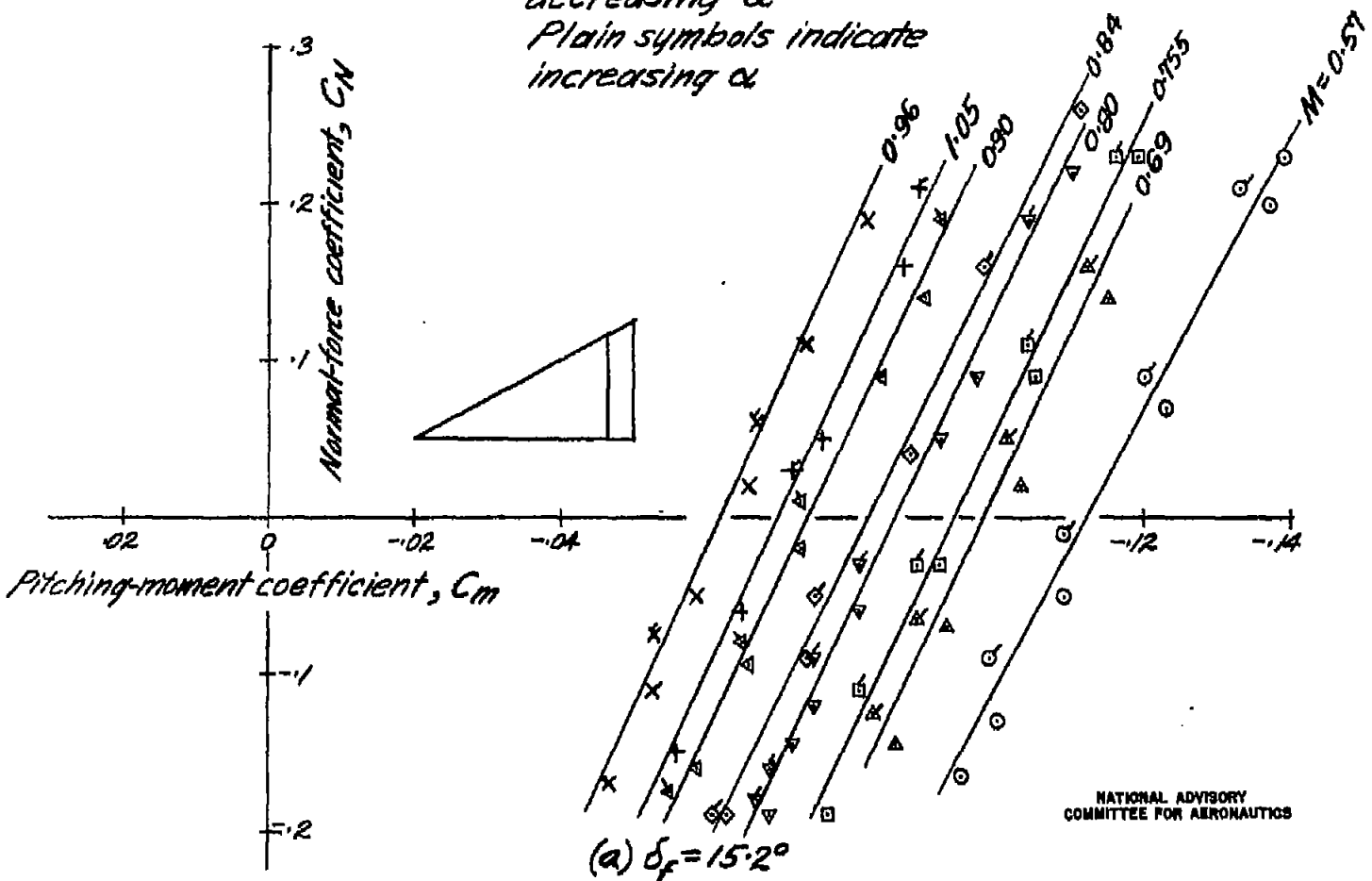

(a) $\delta_f = 15.2°$

Figure 11. ——— Variation of pitching-moment coefficient with normal-force coefficient at various Mach numbers for triangular wing with constant-chord flap.

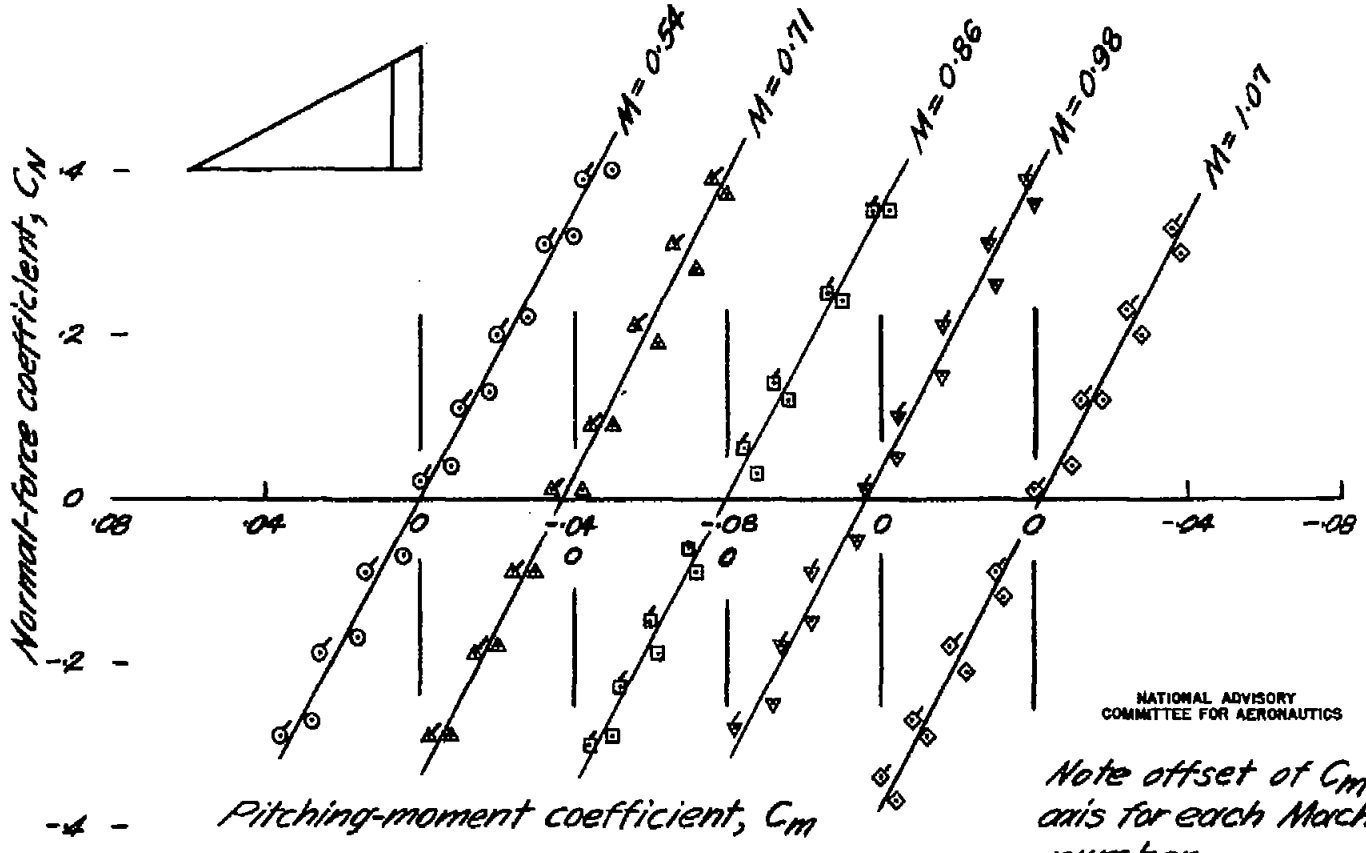

(b) $\delta_f = 0°$

Figure 11. —— concluded.

[redacted]

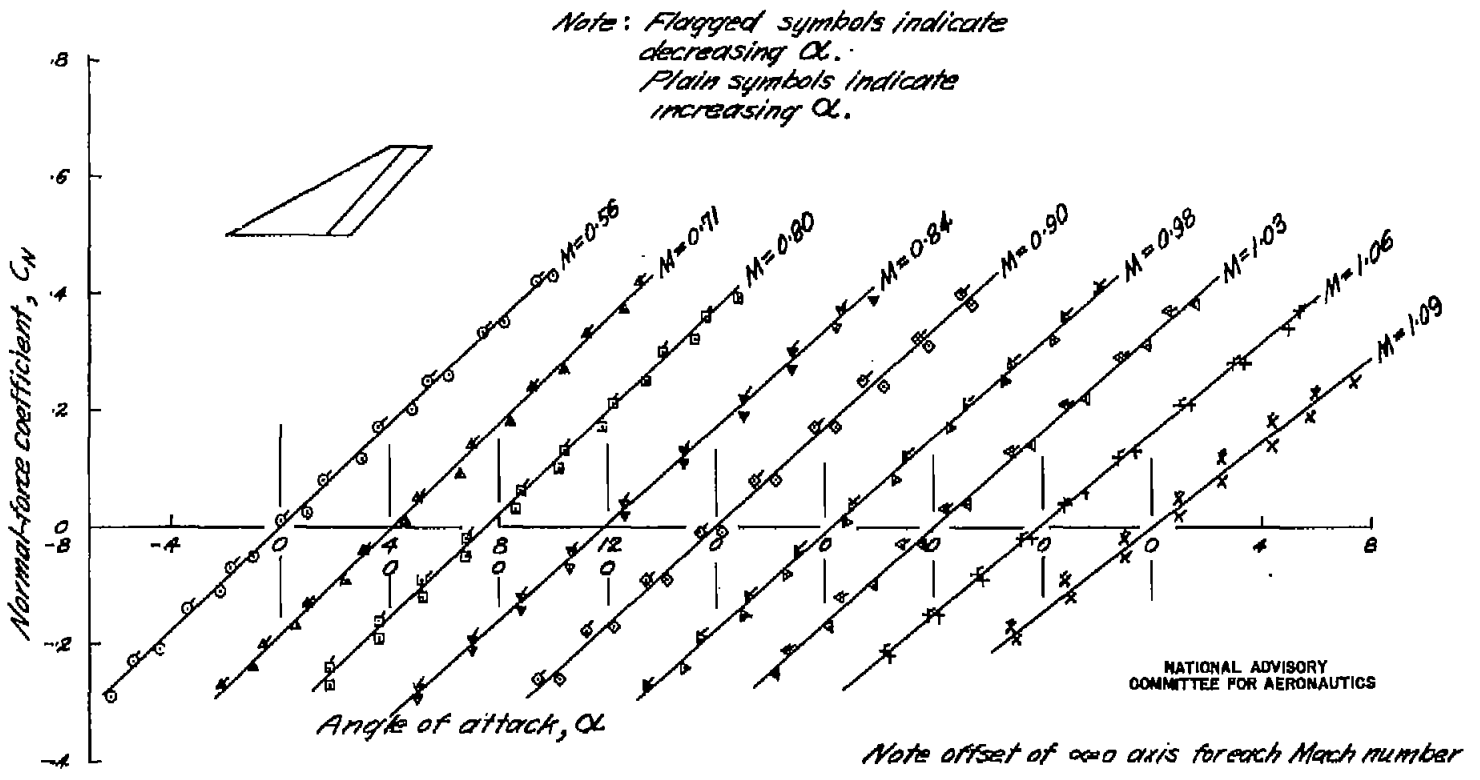

Figure 12. —— Variaton of normal-force coefficient with angle of attack at various Mach numbers for swept-back planform, $\delta_f = 0°$.

[redacted]

~~CONFIDENTIAL~~

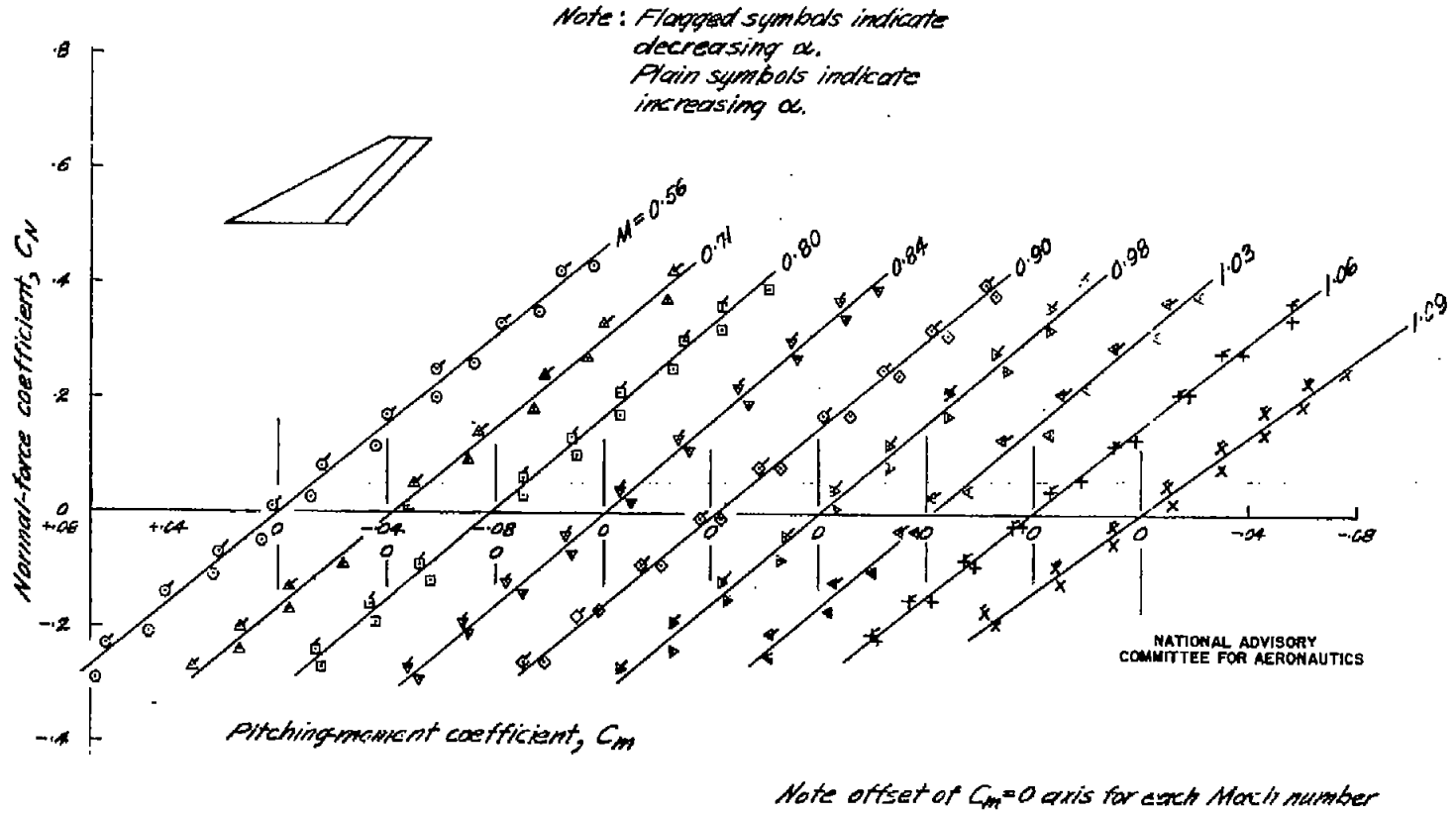

Note offset of $C_m = 0$ axis for each Mach number

Figure 13. ——— Variation of pitching-moment coefficient with normal-force coefficient at various Mach numbers for swept-back planform, $\delta_f = 0°$.

~~CONFIDENTIAL~~

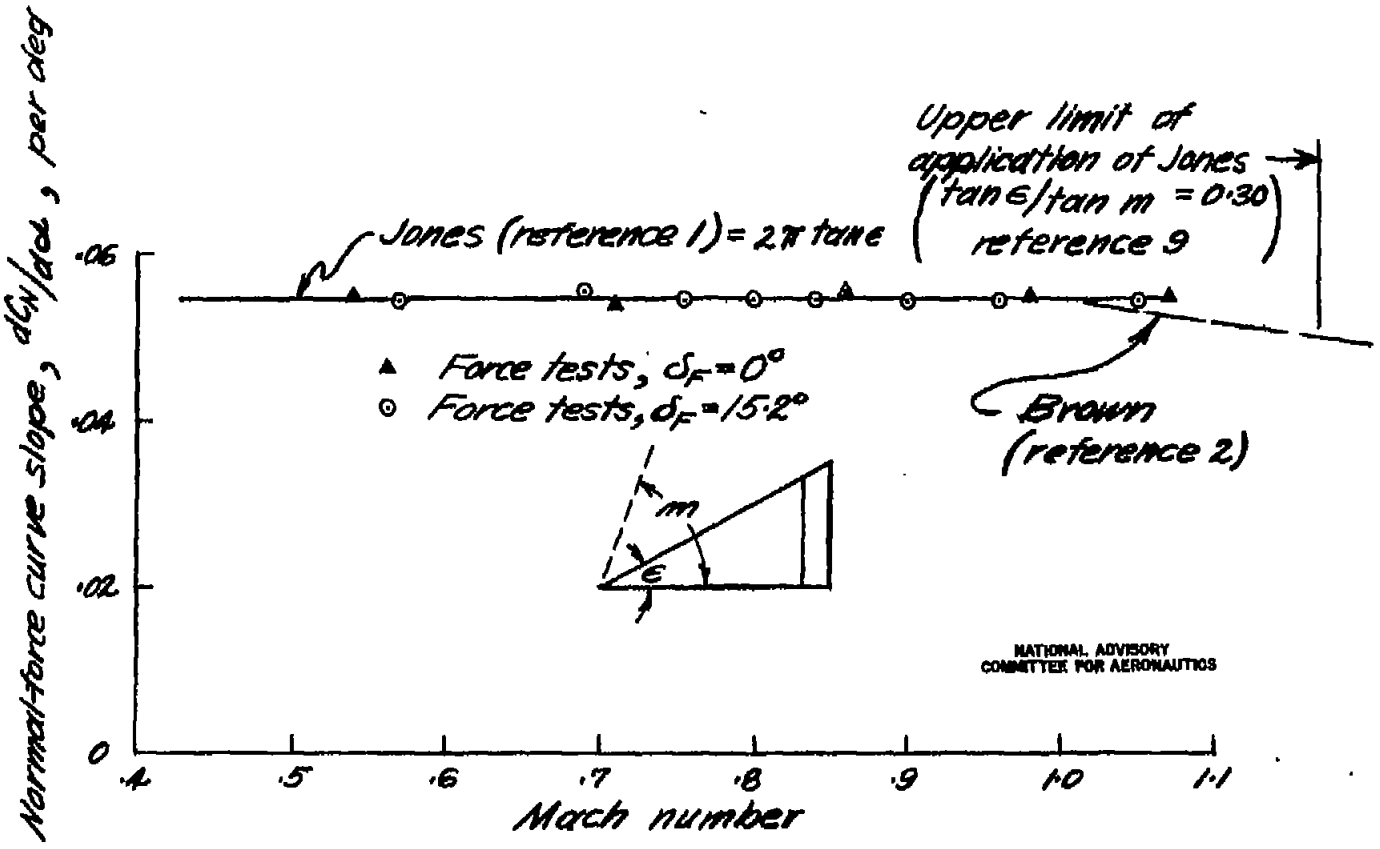

Figure 14.—— Variation of normal-force curve slope with Mach number for triangular wing, A=2, showing effect of flap deflection and comparison with theory.

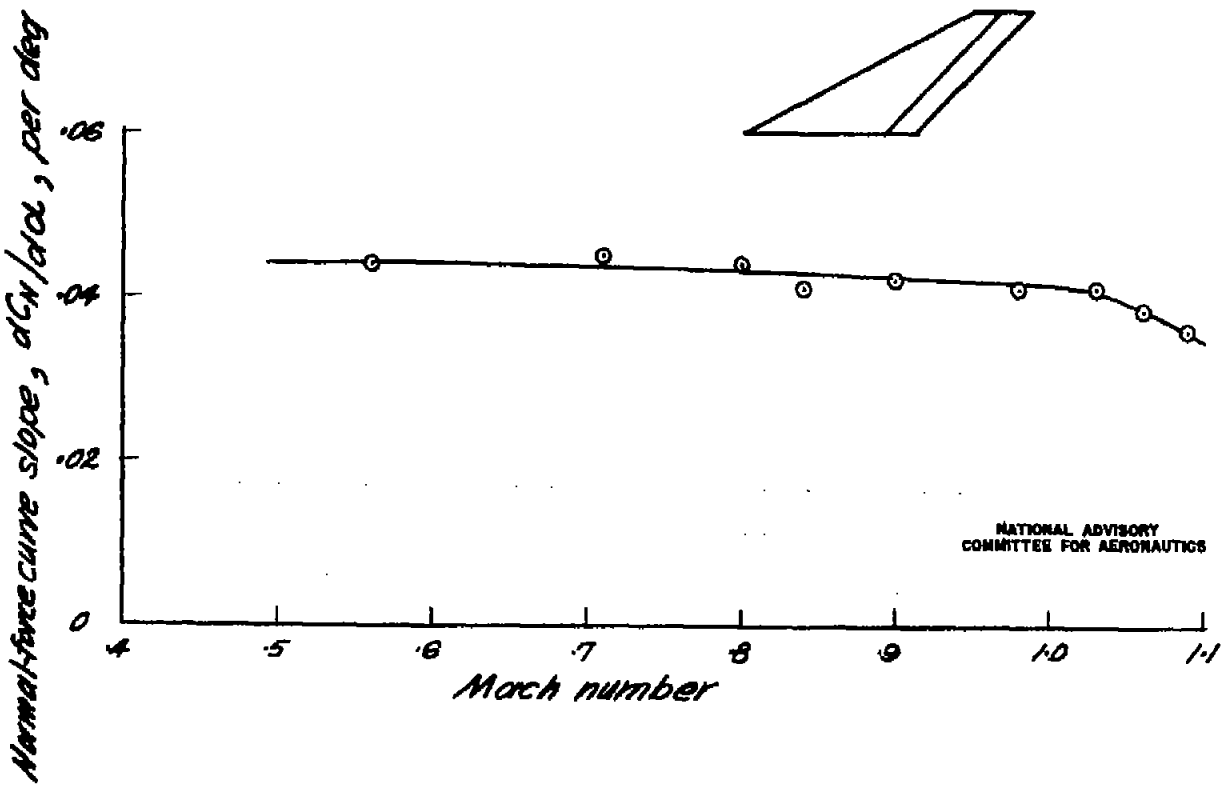

Figure 15. —— Variation of normal-force curve slope with Mach number for swept-back planform, $A = 2$, $\delta_f = 0°$.

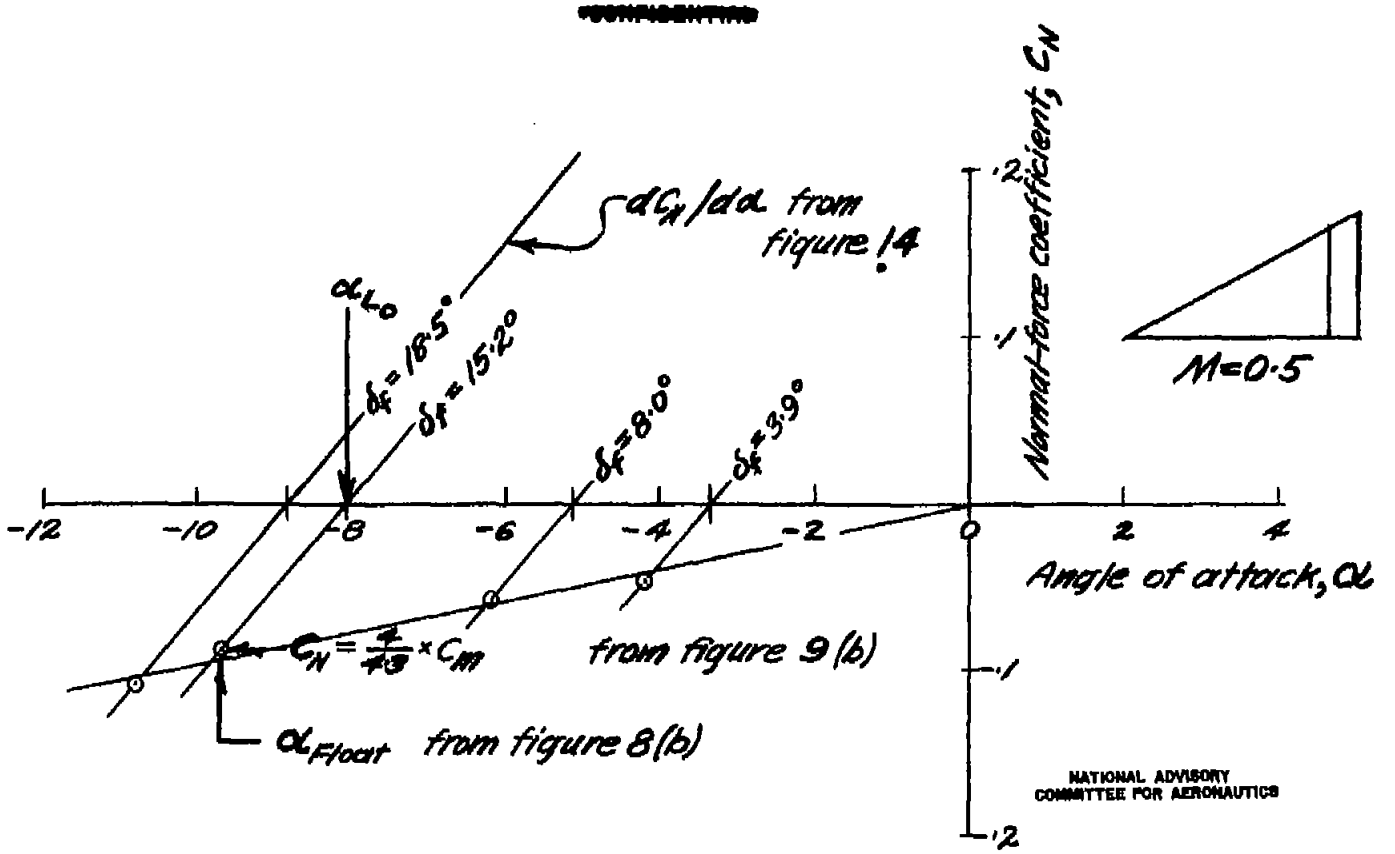

Figure 16. —— Graphical illustration of method of correcting α_{Float} to α_{L_0}, using constant-chord flap at M = 0.5 as example.

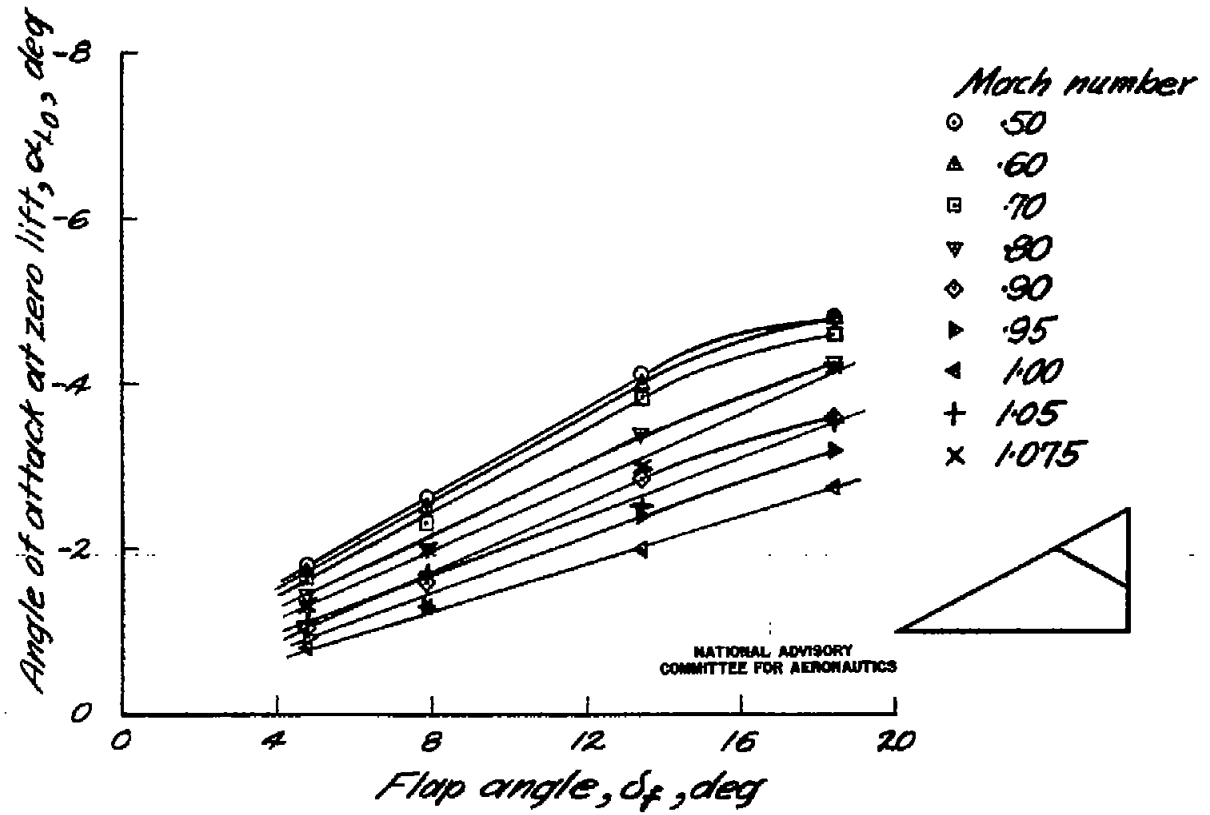

(a) Triangular drooped-tip flap

Figure 17. — Variation of angle of attack at zero lift with flap angle for various Mach numbers.

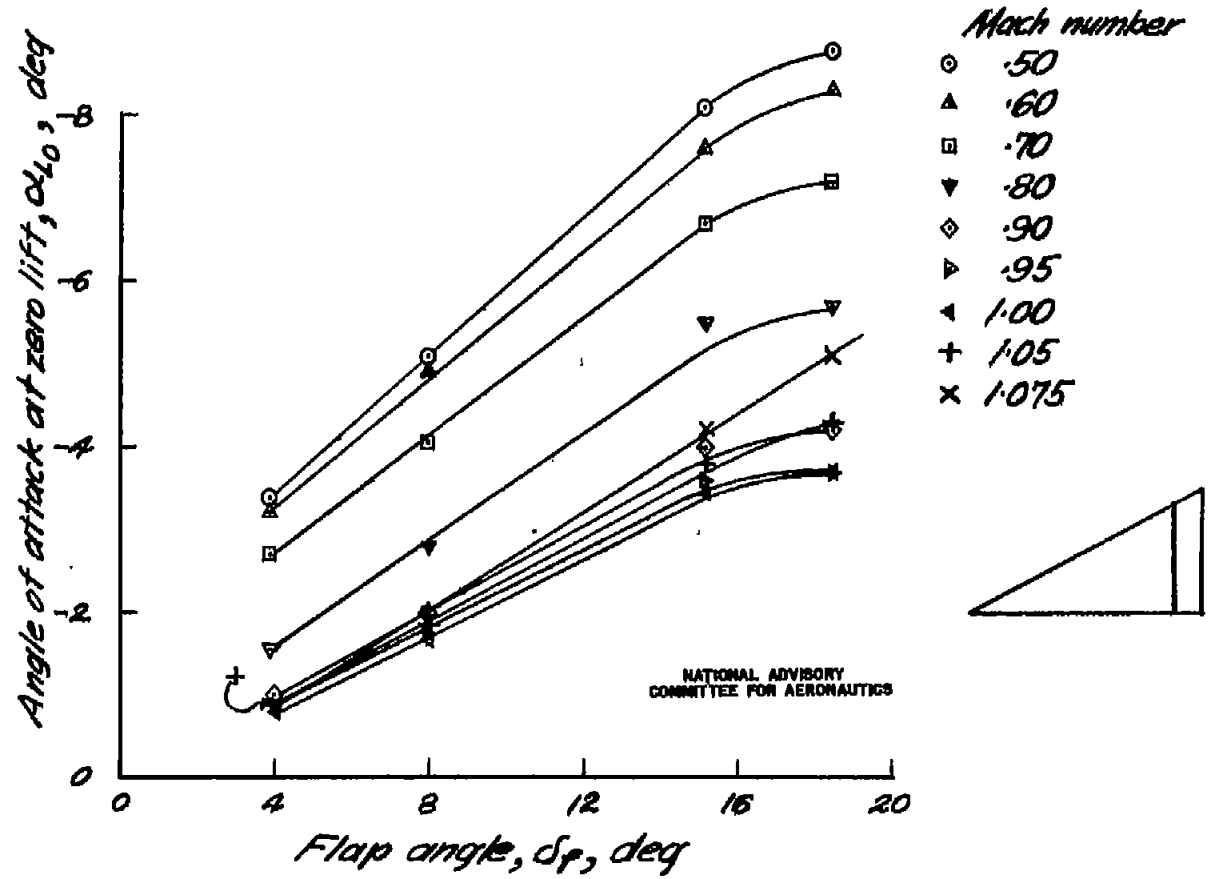

(b) Constant-chord flap

Figure 17. — continued

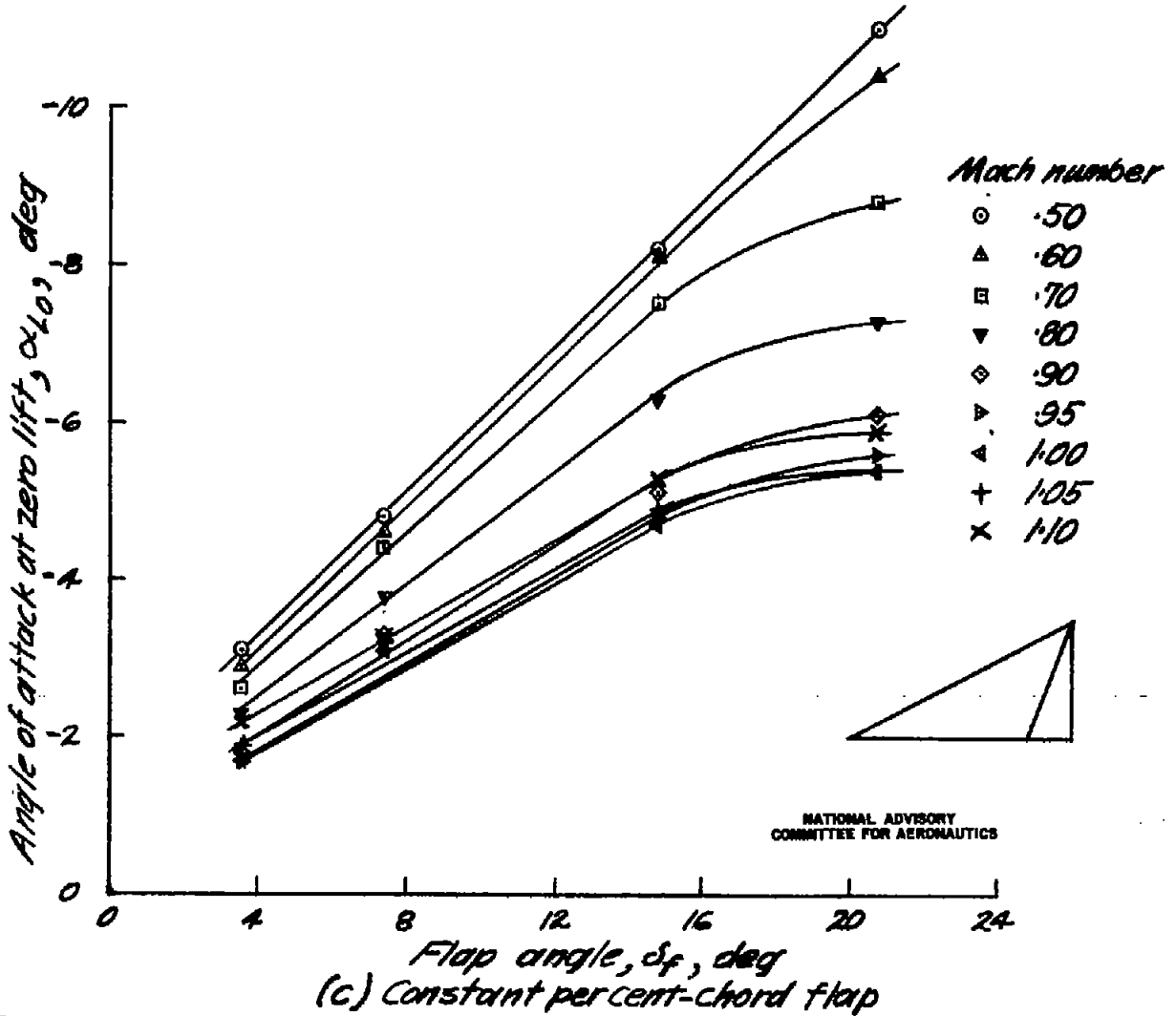

(c) Constant percent-chord flap

Figure 17. —— continued

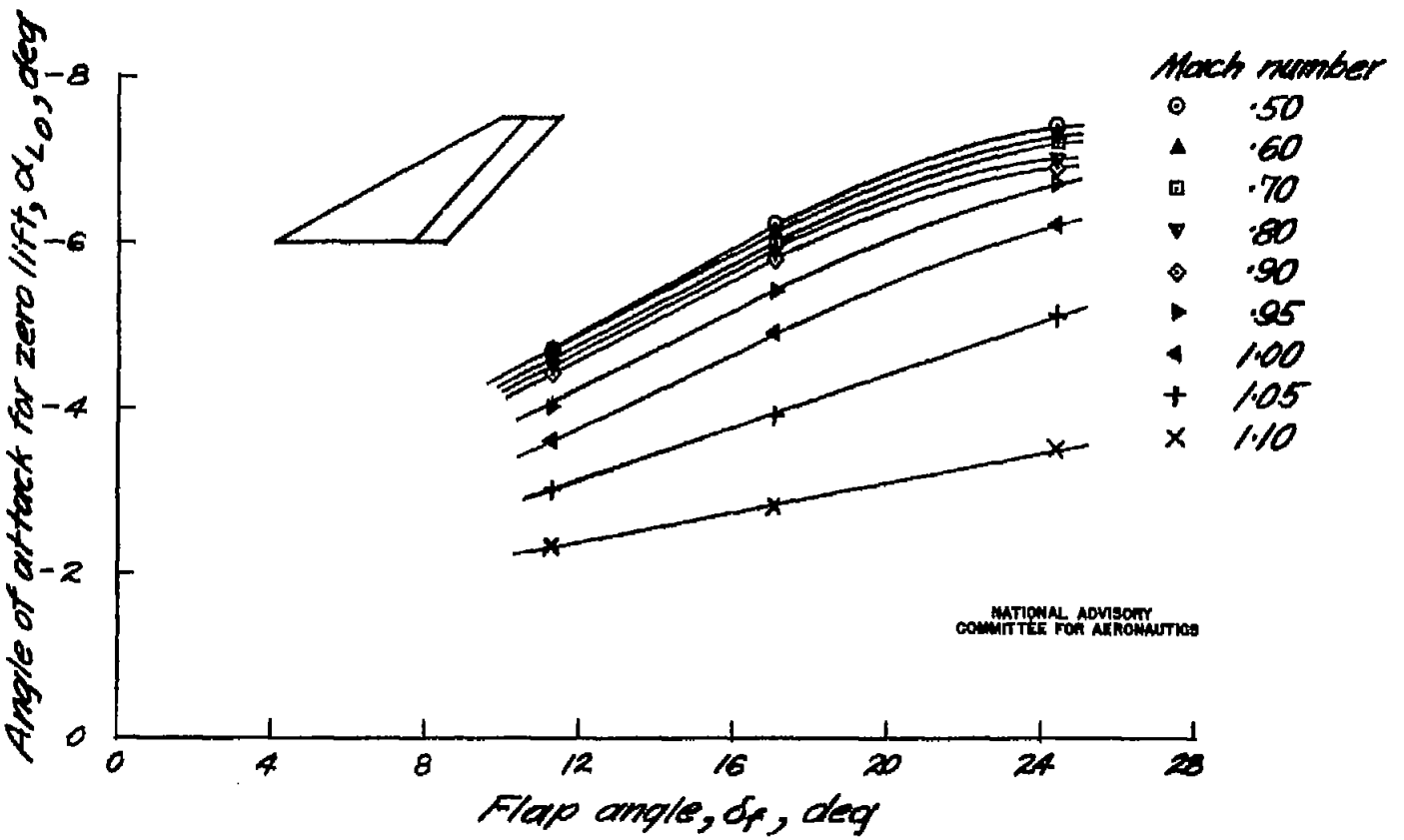

(d) Swept-back constant-chord flap

Figure 17. ——— concluded.

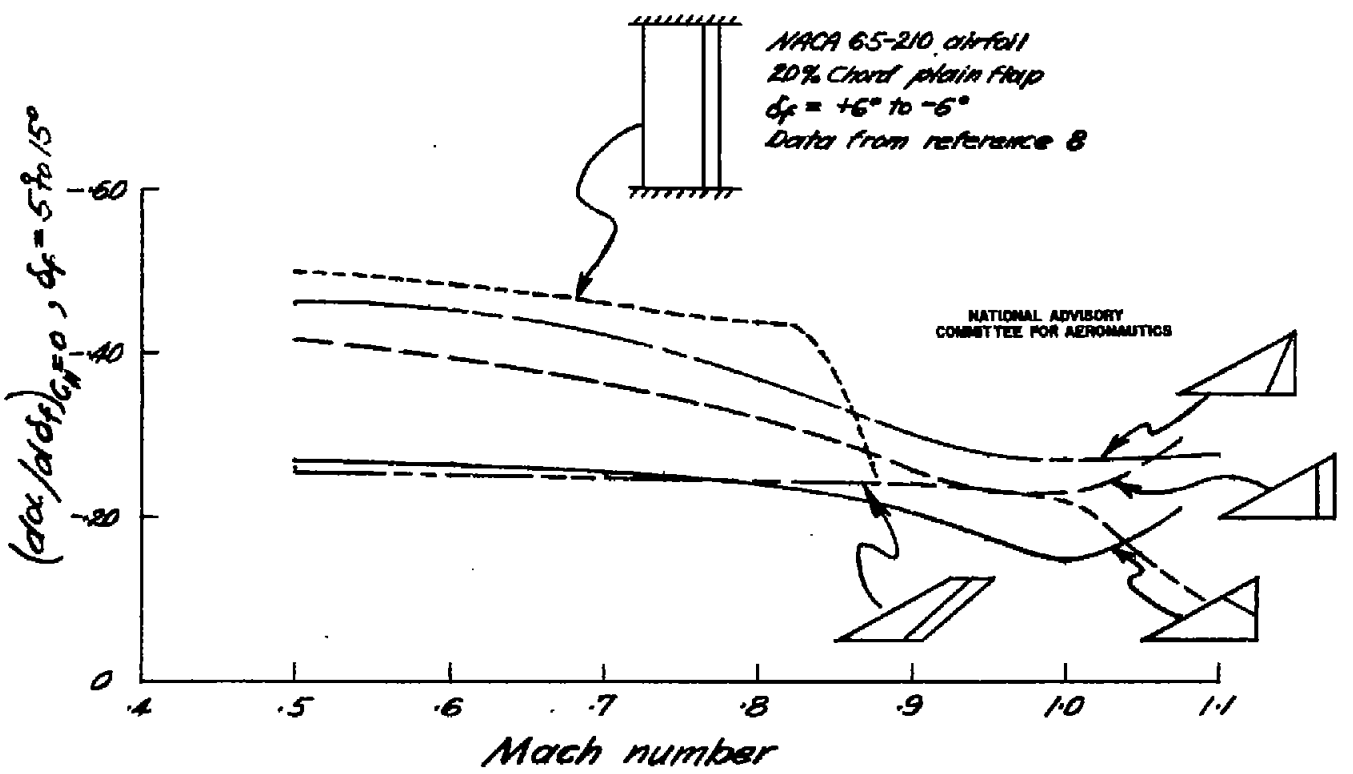

Figure 18. —— Variation of lift-producing effectiveness parameter, $(d\alpha/d\delta_f)_{C_N=0}$, with Mach number for the four control configurations tested, including comparison with straight wing.

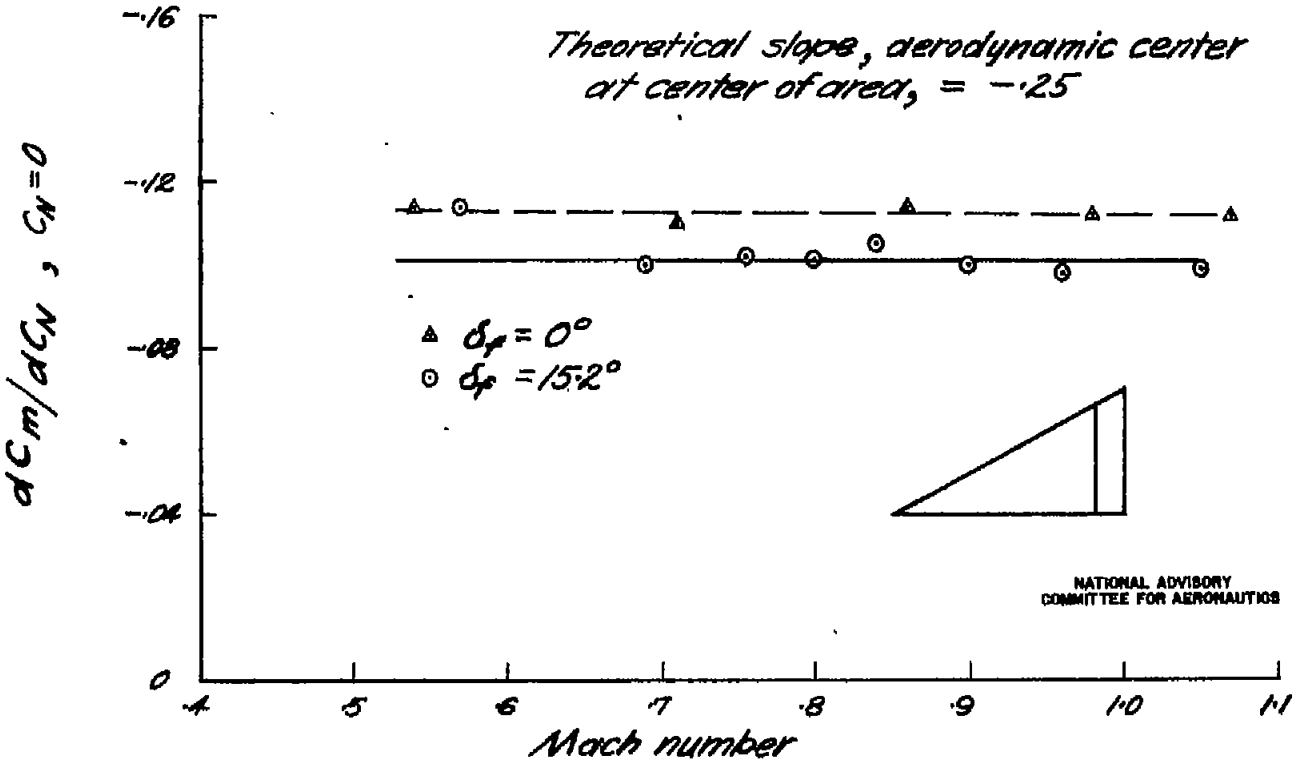

Figure 19. —— Variation of pitching-moment slope with Mach number for triangular wing, A=2, showing effect of constant-chord flap deflection.

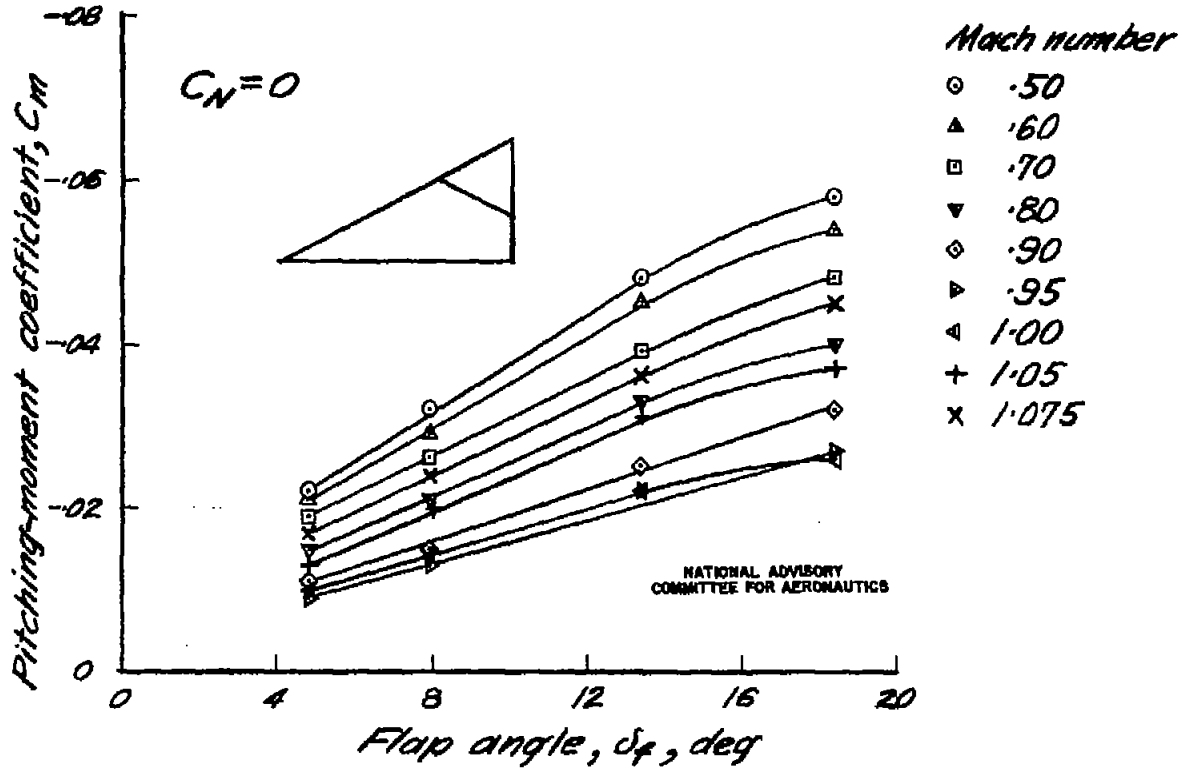

(a) Triangular drooped-tip flap

Figure 20.——— Variation of pitching-moment coefficient at zero lift with flap angle at various Mach numbers.

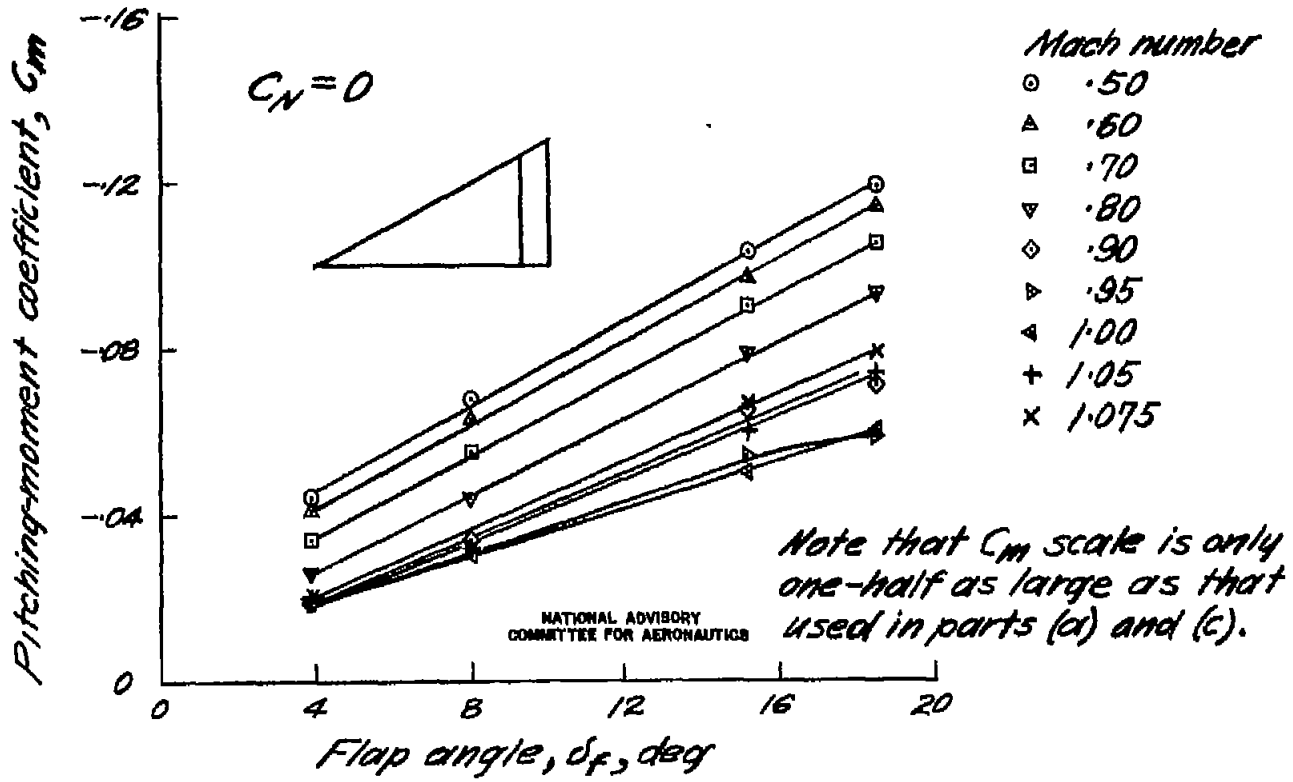

(b) Constant-chord flap

Figure 20. —— continued

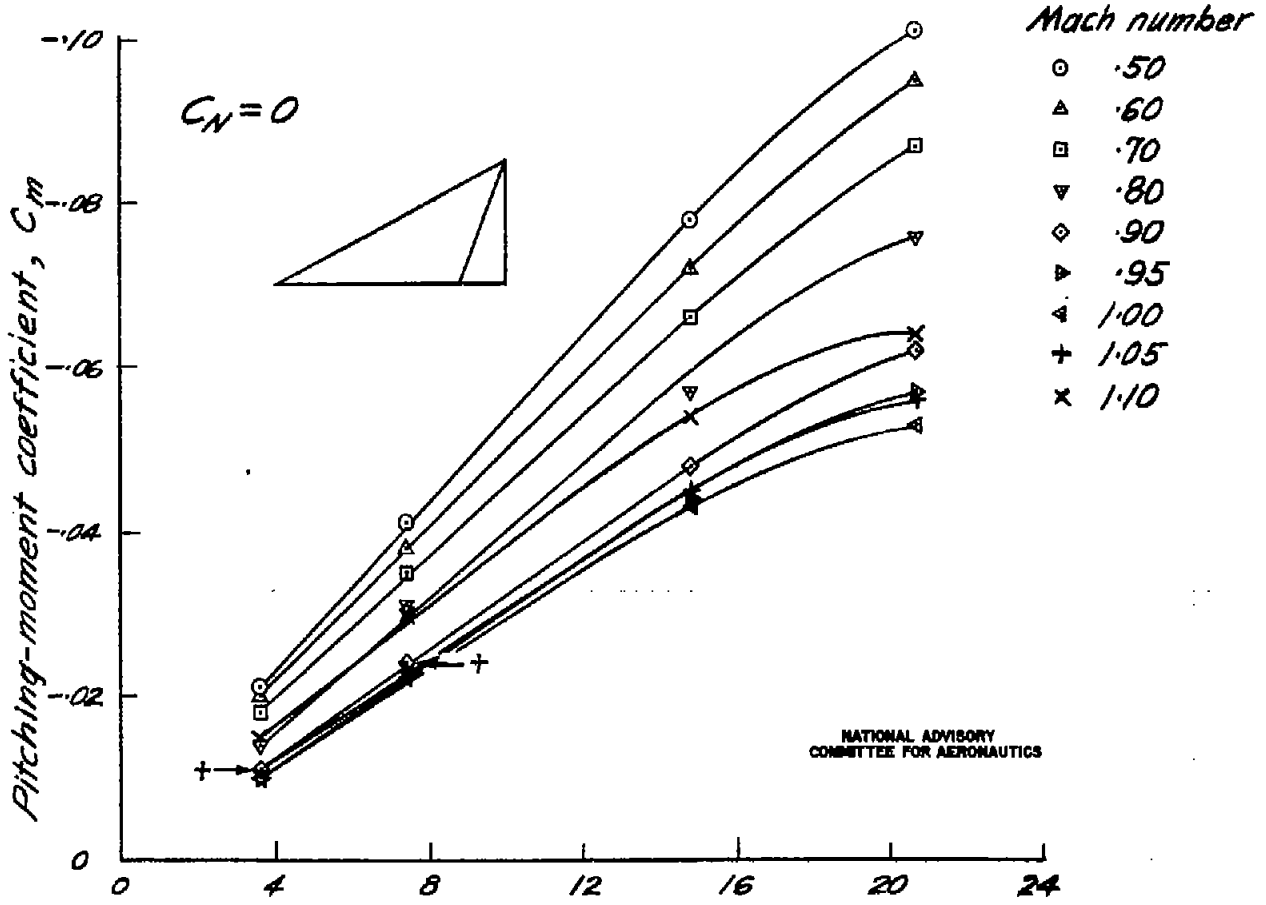

(c) Constant percent-chord flap

Figure 20. —— concluded.

[redacted]

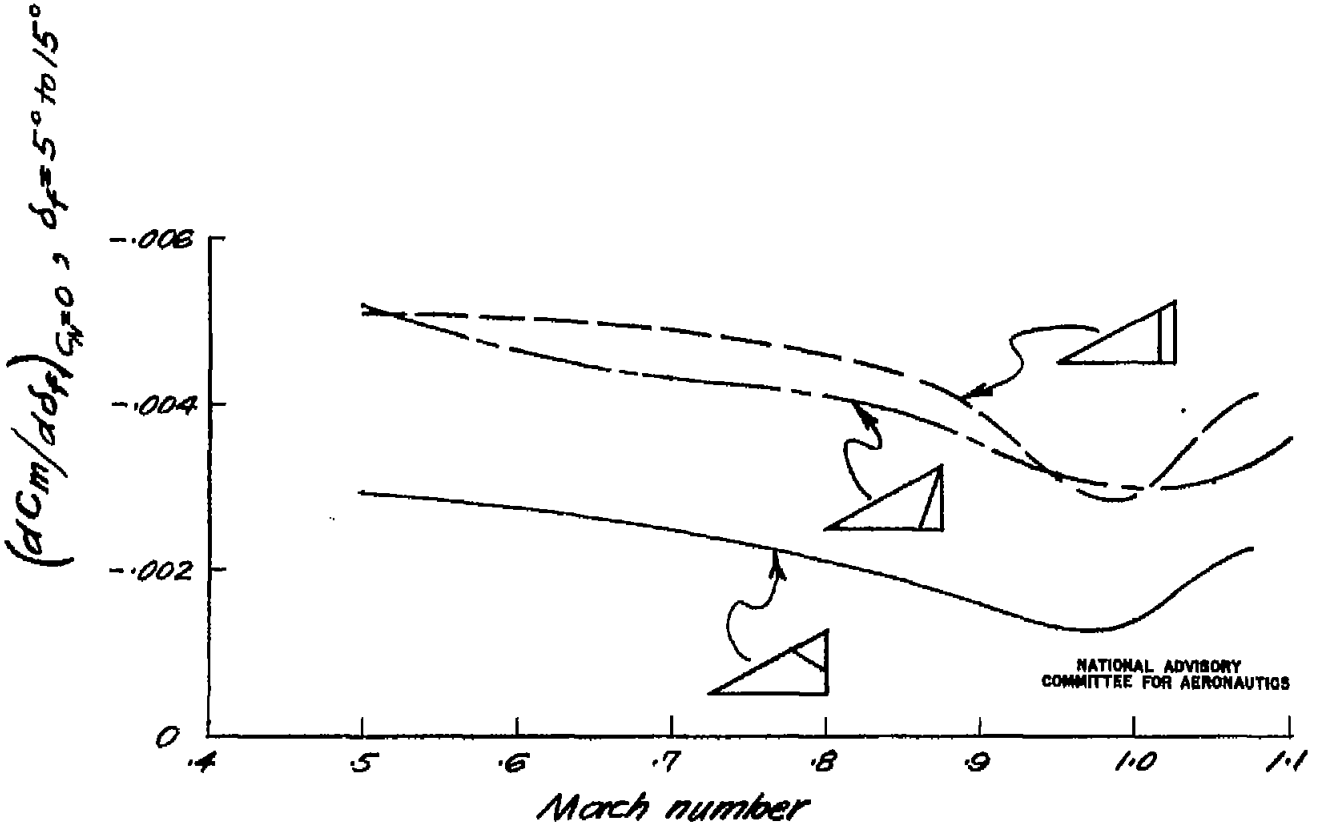

Figure 21. —— Variation of pitching-moment effectiveness with Mach number for the three triangular wing controls. [redacted]

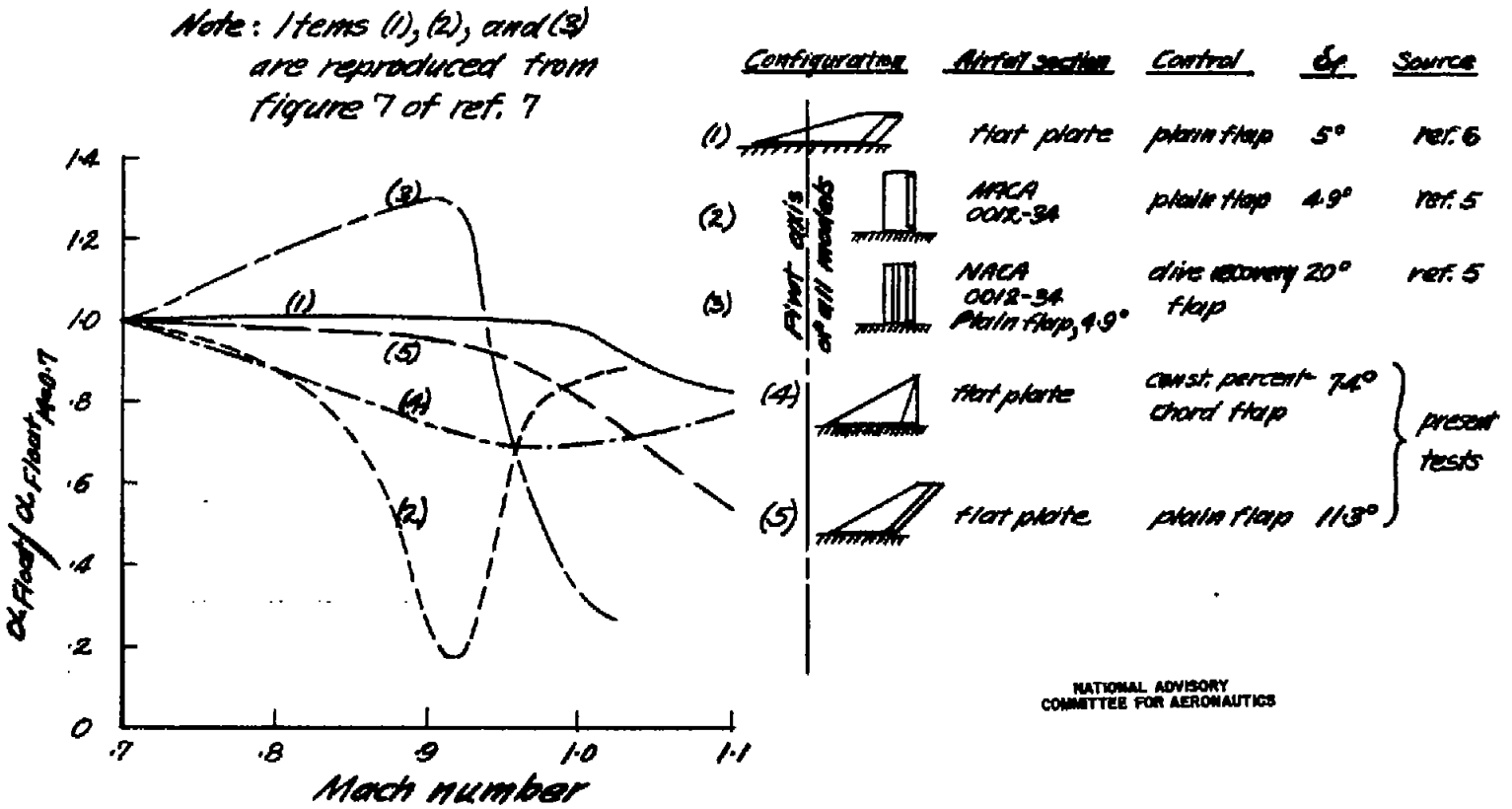

Figure 22. —— Relative effectiveness of several planforms and control surface arrangements as determined by NACA wing-flow method floating angle tests in the transonic speed range.

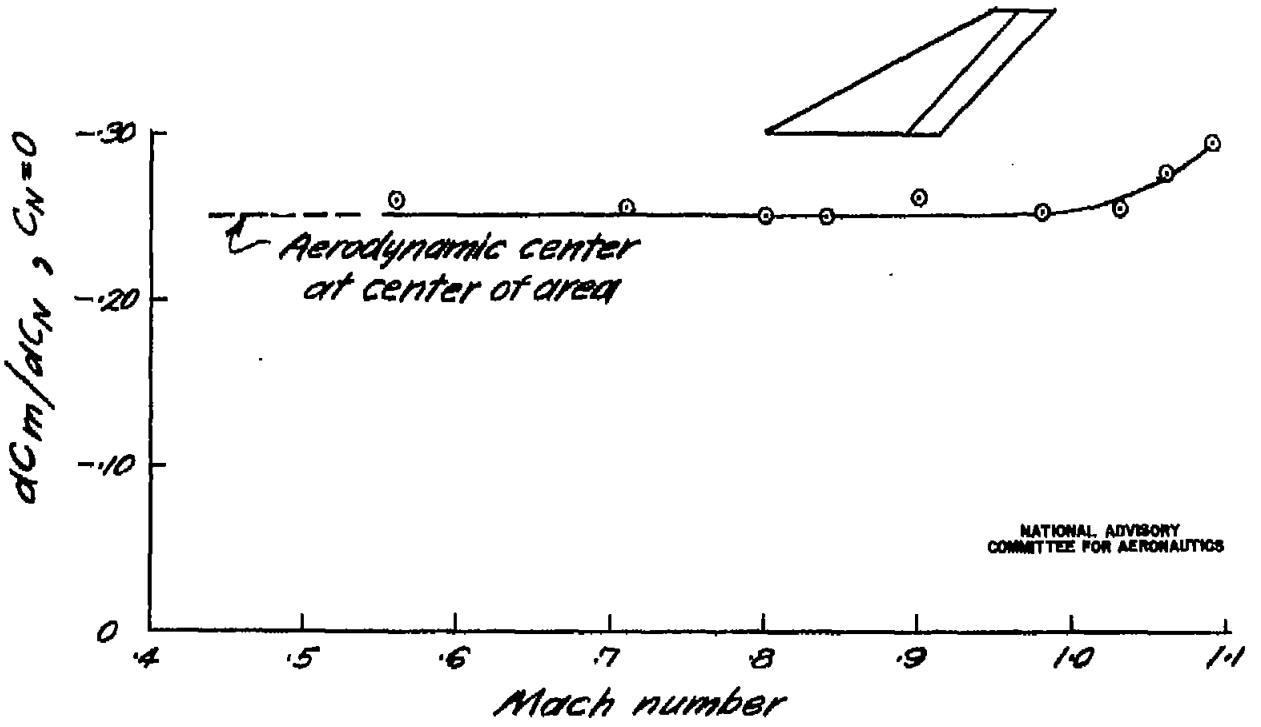

Figure 23. —— Variation of pitching-moment slope with Mach number for swept-back planform, A=2, $\delta_f = 0°$.

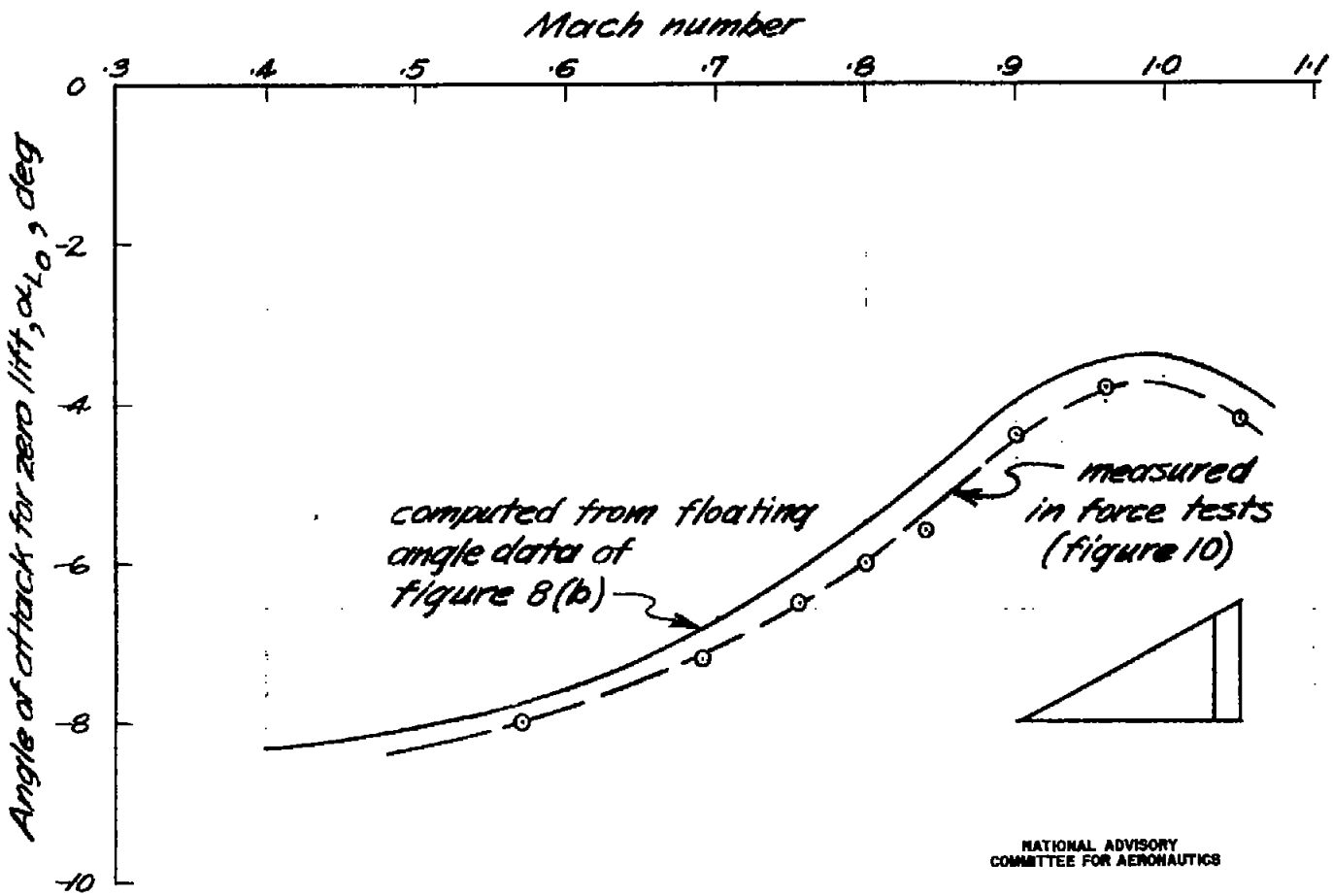

Figure 24. —— Variation of angle of attack for zero lift with Mach number for constant-chord flap, $\delta_f = 15.2°$, comparing results from both test methods.

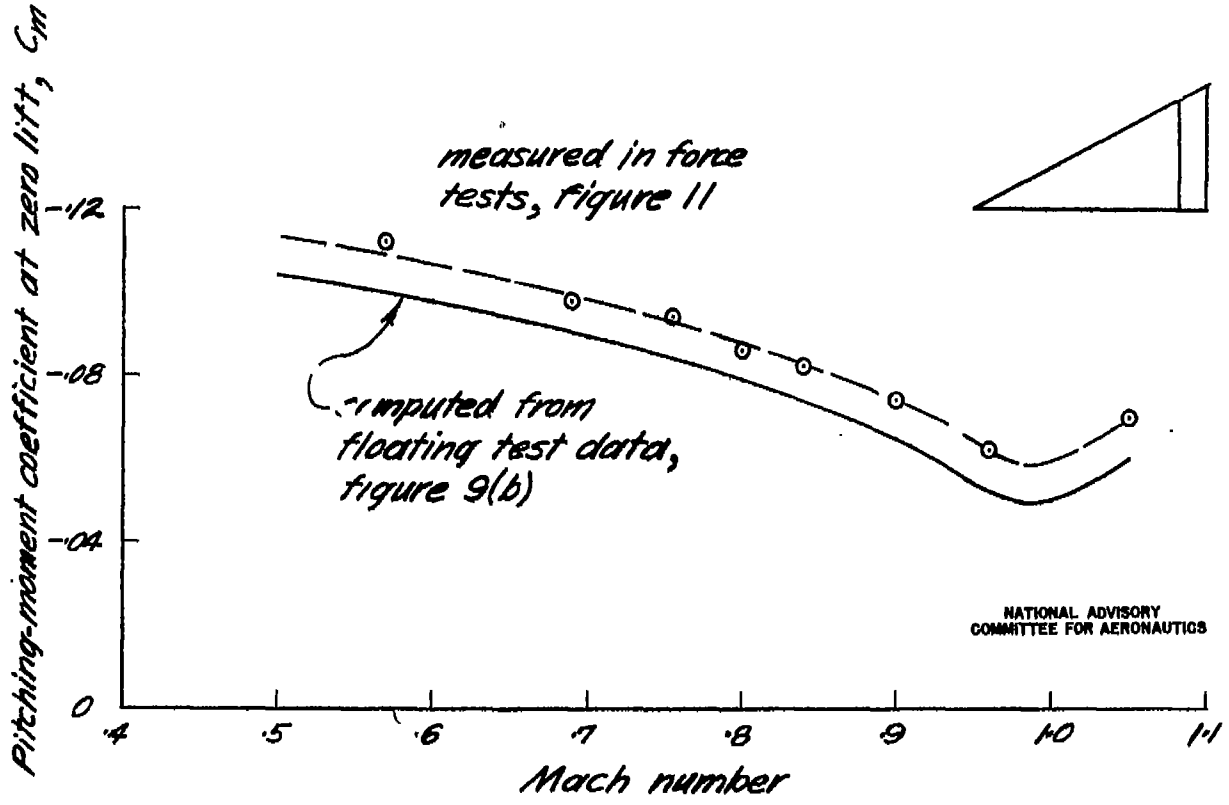

Figure 25. ——— Variation of pitching-moment coefficient at zero lift with Mach number for constant-chord flap, $\delta_f = 15.2°$, comparing results from both test methods.

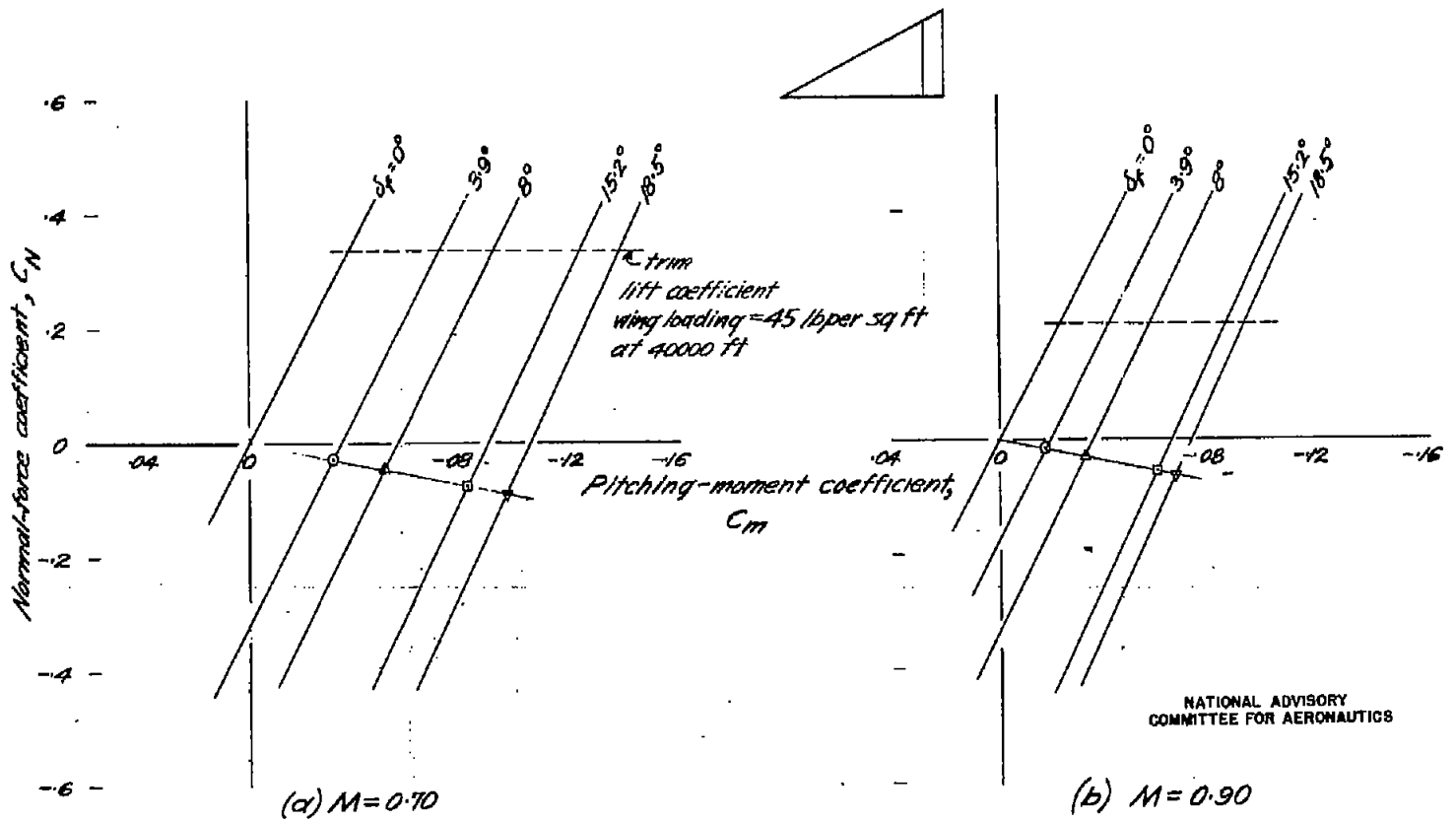

Figure 26. ——— Variation of pitching-moment coefficient with normal-force coefficient at constant flap angle for various Mach numbers, triangular planform with constant-chord flap.

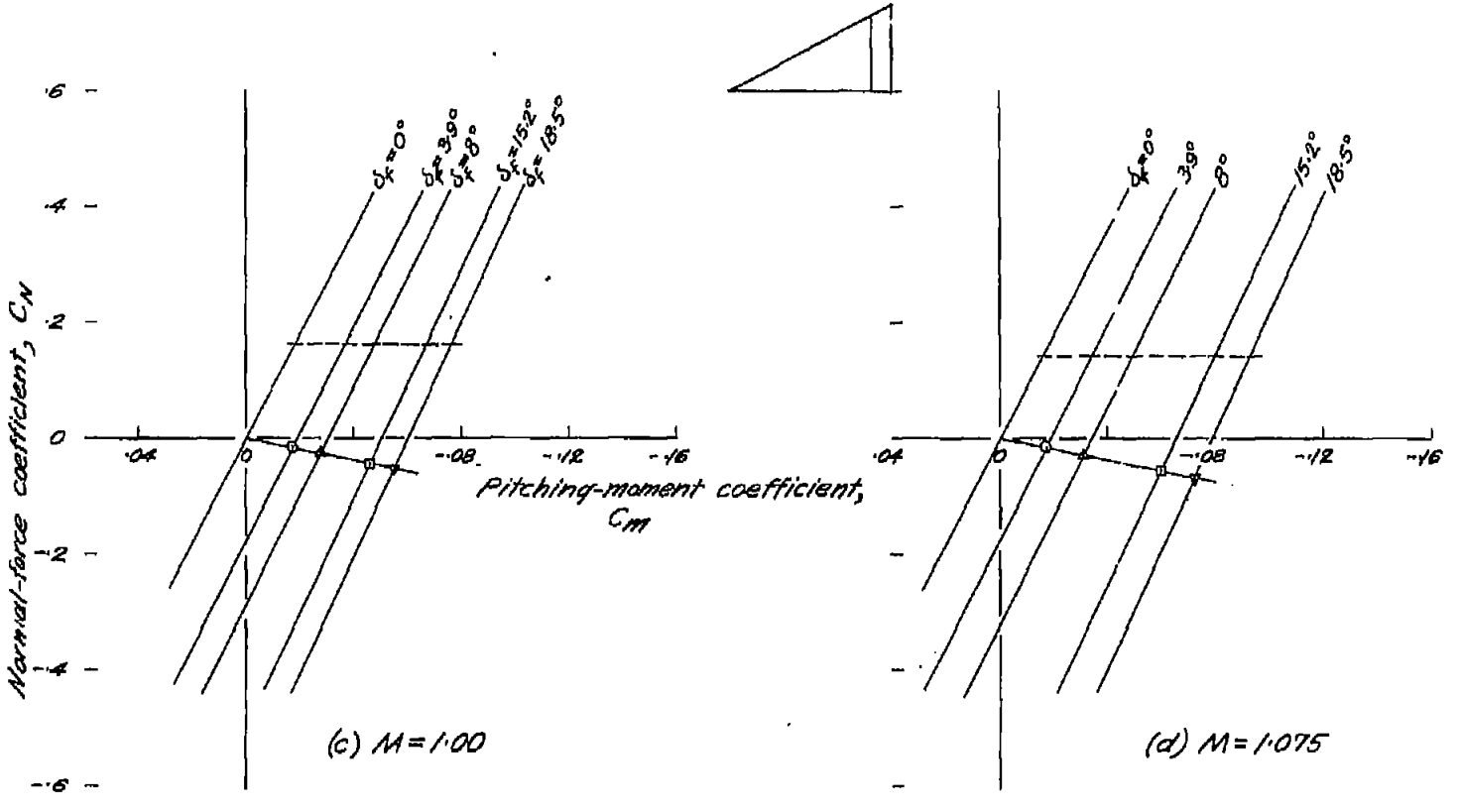

Figure 26. —— concluded.

NATIONAL ADVISORY
COMMITTEE FOR AERONAUTICS

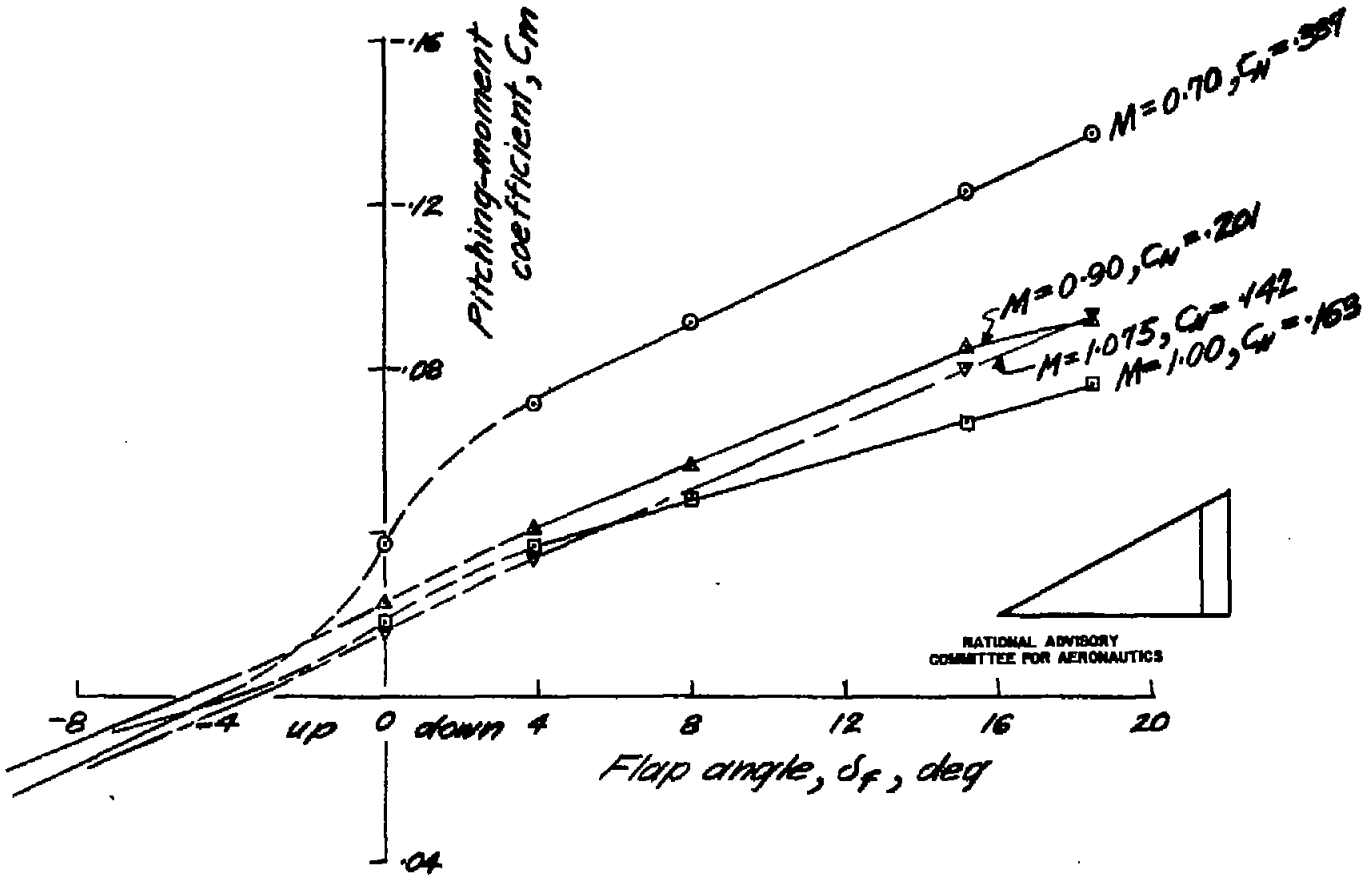

Figure 27. ——— Variation of pitching-moment coefficient with flap angle at specified Mach numbers and normal-force coefficients.